



A novel ENTH domain-containing protein TgTEPSIN is essential for structural maintenance of the plant-like vacuolar compartment and bradyzoite differentiation in *Toxoplasma gondii*

Kai He^{a,b,1}, Ruibin Wu^{a,b,1}, An Yan^{a,b}, Xianyong Liu^{a,b,*}, Shaojun Long^{a,c,**}

^a National Animal Protozoa Laboratory and School of Veterinary Medicine, China Agricultural University, Beijing 100193, China

^b Key Laboratory of Animal Epidemiology and Zoonosis of Ministry of Agriculture, China Agricultural University, Beijing 100193, China

^c Shenzhen Key Laboratory of Pathogenic Microbes and Biosafety, and Laboratory of Zoonotic Diseases, School of Public Health (Shenzhen), Sun Yat-Sen University, Shenzhen Campus, Shenzhen 518107, China



ARTICLE INFO

Keywords:

Toxoplasma gondii
TurboID
PLVAC
ENTH domain
Vesicular transport
Bradyzoite differentiation

ABSTRACT

Toxoplasma gondii is an intracellular and parasitic protozoan that harbors specialized cellular structures and molecular mechanisms, including the Plant-like Vacuolar Compartment (PLVAC). The PLVAC performs multi-faceted roles in the parasite, contributing to ion homeostasis, proteolysis, pH regulation, and autophagy. Despite significant efforts over the past decade to characterize the PLVAC, the proteins localized to this organelle remain largely unidentified. In this study, we utilized TurboID and genetic engineering techniques to uncover additional biological characteristics and the conferring components in the PLVAC. By exploiting the bait PLVAC proteins cathepsin L (CPL) and chloroquine resistance transporter (CRT), we identified 9 novel PLVAC-associated proteins in the compartment. Further essentiality screening reveals that TgTEPSIN is required for the parasite lytic cycle. Further phenotypic analysis demonstrated the depletion of TgTEPSIN resulted in defects in the maintenance of PLVAC, virulence in mice as well as bradyzoite differentiation. Collectively, our findings broaden the repertoire of PLVAC proteins and provide new insights into the essential component and roles of the PLVAC in *T. gondii*.

1. Introduction

Toxoplasma gondii, a highly prevalent parasite in the phylum Apicomplexa, has the ability to infect almost all nucleated cells in diverse mammalian hosts [1]. It plays a significant role in causing congenital disorders and poses serious risks to immunocompromised individuals. It is estimated that this zoonotic parasite affects approximately 30 % of the global population, with an infection rate of 7.88 % in China [2,3]. Additionally, *T. gondii* extensively relies on nutrients and metabolites of host cells, ingesting cytosolic components during the intracellular replication phase [4]. Recent studies have shown that the host cytosolic materials are ingested via the host Endosomal Sorting Complex Required for Transport (ESCRT) machinery at the parasitophorous vacuole membrane (PVM) [5], as well as through a specialized endocytosis

process at the micropore of the parasite plasma membrane (PPM) [6]. Once internalized, these vesicles undergo trafficking processes regulated by prenylated proteins within the parasite cytosol, ultimately reaching the Plant-like Vacuolar Compartment (PLVAC), where the host cytosolic materials are either released or degraded in the acidic environment [6–8].

T. gondii processes a complex endomembrane system that includes the classical eukaryotic organelles, such as the Golgi apparatus and the trans-Golgi network. Proteins destined for secretion through the apical complex organelles, including the micronemes and the rhoptries, typically traffic through these organelles before reaching the early endosomes for further transport [9]. These secretory proteins undergo proteolytic maturation during transport, which is necessary for them to reach their final destinations within the parasite and function correctly

* Correspondence to: X. Liu, Key Laboratory of Animal Epidemiology and Zoonosis of Ministry of Agriculture, China Agricultural University, Beijing 100193, China.

** Correspondence to: S. Long, Shenzhen Key Laboratory of Pathogenic Microbes and Biosafety, and Laboratory of Zoonotic Diseases, School of Public Health (Shenzhen), Sun Yat-Sen University, Shenzhen Campus, Shenzhen 518107, China.

E-mail addresses: Liuxianyong@cau.edu.cn (X. Liu), longshj3@mail.sysu.edu.cn (S. Long).

¹ These authors contributed equally to this work.

[10]. The endocytic pathway involves multiple organelles that become progressively acidic as they mature, with the PLVAC being the most acidic compartment among them [11]. Recent studies have revealed a strong link between the acidic environment of PLVAC and both protein secretion and the maturation of micronemes [12,13]. The trafficking of rhoptry and microneme proteins within *T. gondii* appears to be mediated by TgRab5A and C, suggesting that both types of secretory proteins share the same endosomal transport system. Additionally, a study on TgVHA1 showed that precursor proteins of micronemes and rhoptries can be processed and matured in the ELCs before being transported to their respective secretory organelles, further highlighting the central role of the PLVAC in the endosomal system [13]. These findings suggest that *T. gondii* integrates its endocytic and secretory pathways within its elaborate endomembrane machinery, facilitating the formation of secretory organelles and the regulation of the endocytic system.

It has now been 14 years since the discovery of the PLVAC organelle, which was first characterized using Cathepsin Protease L (TgCPL) staining [14]. Since then, numerous functional proteins have been identified within this organelle. TgCPL localizes to the lumen of PLVAC and plays a crucial role in the maturation of the micronemes and the activation of other PLVAC proteases, such as Cathepsin Protease B (TgCPB) and Aspartyl Protease 1 (TgASP1) [15,16]. The PLVAC contains several hydrolases and shares functional similarities with plant lytic vacuoles [17]. Recent studies have identified several proteins with plant-like characteristics in the PLVAC, including vacuolar H⁺-ATPase (TgVHA1) [13], vacuolar H⁺-pyrophosphatase (TgVP1) [12], and tonoplast intrinsic proteins (TIP)-like aquaporins (TgAQP1) [18]. Additionally, the PLVAC harbors various ion channels and transporters, including those for zinc (TgZnT) [19], iron (TgVIT) [20], Na⁺/H⁺ exchanger (TgNHE3) [21], Ca²⁺/H⁺ exchanger [22,23], phosphate transporter (TgPiT) [24], amino acid transporter (TgAAT1) [25] and chloroquine resistance transporter (TgCRT) [26–28]. Interestingly, TgCRT exhibits a perfect co-localization with TgCPL in *T. gondii*, but is distributed in the membrane structure of the PLVAC, and functions as a key transporter responsible for the translocation of small nutrient molecules. Collectively, these fundamental details illustrate that the PLVAC is involved in the maturation of secretory proteins, ion storage, endocytosis, exocytosis, and autophagy, highlighting the multiple and dynamic roles of the organelles in parasite physiology and pathogenesis. However, open questions regarding to the PLVAC, particularly concerning the vesicle transport and fusion, the formation and maintenance of the acidic environment, and the involvement of the organelles in the maturation of secretory proteins.

In this study, we first investigated the protein composition of the PLVAC by fusing TgCPL and TgCRT with the efficient proximity labeling enzyme TurboID, from which we discovered 9 novel PLVAC proteins. Several proteins are predicted to be involved in vesicle-mediated transport, transporters, and phospholipid metabolic processes. Detailed analysis revealed that depletion of a novel ENTH domain-containing protein TgTEPSIN resulted in defects in the processing of microneme proteins and the ingestion of host cytosolic material marker GFP. These defects were likely caused by the structural disruption of the PLVAC and its lysosomal characteristics, as demonstrated by staining. Furthermore, TgTEPSIN depletion led to a marked defect in parasite differentiation from tachyzoite to the bradyzoite in the alkaline environment. Collectively, our findings identified novel insights into the components of the PLVAC, and highlighted TgTEPSIN as a key PLVAC-associated player in the parasite lytic cycle.

2. Materials and methods

2.1. Ethics statement

In the study, the production of polyclonal antibodies was conducted in compliance with ethical standards and animal welfare needs. The mouse experiments received approval from the Veterinary Office of

China Agricultural University (Approval No. AW11402202-2-1). Mice were euthanized using a CO₂ overdose to ensure a humane process.

2.2. Antibodies and chemical reagents

This study employed a variety of primary antibodies, including commercially sourced options like mouse anti-HA (BioLegend, #901501) and rabbit anti-HA (Thermo-Fisher, #71-5500), and several in-house antibodies, such as rabbit anti-GRASP (Golgi Reassembly and Stacking Protein), rabbit anti-HSP60 (Heat Shock Protein 60), rabbit anti-STX6 (Syntaxin 6), rabbit anti-IMC1 (Inner Membrane Complex Protein 1), rabbit anti-Tubulin, rabbit anti-ACP (Acyl Carrier Protein), rabbit anti-Centrin1. Antibodies of mouse mAb 6D10 anti-MIC2 (Microneme Protein 2), mouse anti-Ty (BB2), rabbit anti-ROP5 (Rhoptry Protein 5) are generous gifts from the David Sibley lab. Secondary antibodies including anti-mouse and anti-rabbit antibodies conjugated with Alexa Fluors (488, 350 or 568) were obtained from Thermo-Fisher Scientific. Fluorescent antibodies conjugated with LICOR 680CW and 800CW were purchased from LICOR. In addition, other chemicals purchased from Sigma-Aldrich supplier include Lyso-Tracker Red (#SCT138), D-biotin (Sigma-Aldrich, no. B4639), 3-indoleacetic acid (IAA/auxin) (#M3536), 6-xanthine (6-XA, #X4002), calcium ionophore A23187 (#C7522), pyrimethamine (Pyri, #46706) and mycophenolic acid (MPA, #M3536).

2.3. Parasites and host cell culture

The Parasites lines RHΔhxgprtΔku80, RHΔhxgprtΔku80/TIR1, and ME49ΔhxgprtΔku80/TIR1 were referred to as RH, TIR1 and ME49 in the study, respectively. These strains, along with their derived variants (Table S1A), were maintained in culture using human foreskin fibroblast HFF-1 cells. The parasites lines were grown in D5 medium (DMEM supplemented with 5 % fetal bovine serum). Both parental lines and transgenic strains were propagated in vitro via serial passage in monolayers of HFF-1 cells, with mycoplasma-negative conditions, as previously described [29]. For the subsequent experimental assays, the TIR1 and AID strains were treated with 500 μM auxin (+IAA) or 0.1 % ethanol alone (-IAA) as a control, following the protocols outlined in earlier reports [30,31].

2.4. Plasmids and strains

All plasmids and corresponding primers used in the study are listed in Table S1B and Table S1C, respectively. These generic tagging plasmids included pNL-TurboID-4Ty-DHFR, pN-6Ty-HXGPRT, pL-6Ty-DHFR, pNL-6HA-HXGPRT, pL-6HA-DHFR and pL-AID-6Ty-DHFR. For the construction of different mutant strains, the optimal sgRNA sequences targeting specific regions were selected using the online tool EuPaGDT (<http://grna.ctegd.uga.edu/>), which were incorporated into primers, and subsequently cloned into the pSAG1::Cas9-U6::sgUPRT plasmid (Addgene #54467). To facilitate integration at the Double-Strand Break (DSB) sites obtained by the Cas9 and specific sgRNA, the tagging amplicon generated from generic tagging plasmid was endogenously incorporated into the targeting area at the DSB by homologous regions in the amplicons. Briefly, for the construction of AID parasites lines, the pL-AID-6Ty-DHFR plasmid was used as a template to produce an amplicon for integration of the AID-Ty cassette at the targeted gene in *T. gondii*. The amplicon produced from these plasmids using primers L and T contains two 41 bp regions of homology: one upstream (HR1) near the stop codon and another downstream (HR2) adjacent to the Cas9 cleavage site. These homologous regions enable the in-frame insertion of epitope tags into target genes. The resulting *T. gondii* lines were subjected to drug selection and subcloning, followed by validation through diagnostic PCR, immunofluorescence assays (IFA).

2.5. Transfection and selection

Approximately 1×10^7 freshly egressed parasites were mixed with 10–20 µg of the pCas9-sgRNA plasmid and 2–5 µg of the corresponding amplicon in 250 µL Cytomix buffer (25 mM HEPES, 2 mM EDTA, 10 mM KPO₄, 120 mM KCl, 5 mM MgCl₂) using a 4-mm gap BTX cuvette. This mixture was then electroporated via the BTX ECM 830 electroporator (Harvard Apparatus) according to an established protocol [32]. The transfected tachyzoites were then cultured on HFF monolayers, and after 24 h, selective drugs were applied using either 25 µg/mL MPA, 50 µg/mL 6-XA, or 3 µM Pyri. Subsequently, positive selection pools were diluted and subcloned into 96-well plates at a density of three parasites per well, followed by culturing in the wells for 7 days. Wells exhibiting a single plaque were identified, and pure clones were verified via diagnostic PCR and IFA analysis with the specific antibodies.

2.6. Immunofluorescence and colocalization

Immunofluorescence analysis (IFA) was conducted on the coverslip of 24-well plate with coverslips. One hour later, uninvaded parasites were removed with PBS washes. At 24 h post-infection, coverslips were fixed using 4 % paraformaldehyde for 20 min, then permeabilized using 2.5 % Bovine Serum Albumin (BSA) and 0.25 % Triton X-100 for 20 min. Various combinations of primary antibodies were first used to incubate these coverslips for 40 mins, followed by a 30-min incubation with corresponding secondary antibodies. The coverslips were washed 5 times with BSA containing 0.05 % Tween-20. The coverslips were then mounted on ProLong Gold Antifade Mountant with or without DAPI (36,930 and 36,931, Thermo Fisher Scientific). Parasites were visualized using a Nikon confocal Ni-E C²⁺ microscope, followed by co-localization analysis of the Pearson correlation coefficient (PCC) values using NIS Elements AR software.

2.7. SDS-PAGE and immunoblotting

For western blot analysis, freshly released parasites from syringe-lysed HFF cells were resuspended in PBS and lysed using 5× Laemmli sample buffer with 1 mM DTT, followed by boiling at 98 °C for 10 min. Protein samples were loaded onto precast 10 % SDS-PAGE gels for separation and subsequently blotted using a BioRad wet-blotting system. After blocking process, the different combinations of primary antibodies diluted at 1:1000 were used to incubate the membranes at 4 °C, followed by incubation with corresponding secondary antibodies. Finally, immunoreactive bands were imaged using the Bio-Rad ChemiDOC MP imaging system.

2.8. Affinity purification of biotinylated proteins

The constructed TurboID strains were cultured for 24 h and then treated with 500 µM D-biotin for 90 min on HFF cells. Prior to the purification, the biotinylated proteins in the parasites were examined using streptavidin reagents in both IFA and western blot procedures. After 36 h of growth, the intracellular and extracellular parasites were all harvested and processed for biotinylated protein purification. Subsequently, parasites were lysed in a buffer containing 0.2 % SDS, 0.5 % deoxycholate and 1 % Triton X-100, followed by sonication using a microtip in a 550 sonic dismembrator. The purification of these biotinylated proteins collected from the cleared lysate supernatant was performed using streptavidin magnetic beads, according to the previously established protocol [33].

2.9. Mass spectrometry and proteomic analysis

After the purification, these biotinylated proteins were separated on SDS-PAGE gels, and then stained with Coomassie Blue R250 and fixed in a solution of 10 % glacial acetic acid and 45 % methanol. After vacuum-

drying of protein lanes, the gels were rehydrated, finely chopped, and treated to wipe off stain and SDS through reduction, alkylation, and washing steps. Each digested sample was then analyzed using a Q Exactive HF mass spectrometer coupled with nanoscale liquid chromatography-tandem mass spectrometry (nanoLC-MS/MS) on a 0.075 × 250 mm C18 column using a 2-h gradient. For protein identification and quantification, the obtained spectra were searched in the *T. gondii* GT1 genome and UniProt database using MaxQuant 1.6.14 software. The normalized quantitative data, also known as intensity values based on the LFQ algorithm, were acquired for subsequent bioinformatics analysis. For the comparison between TurboID lines and the parental line, differentially expressed proteins (DEPs) were defined as those that meet the threshold with a *P*-value ≤ 0.05 and an absolute fold change ≥ 1.5. On this basis, the volcano plot generated by the ‘ggplot2’ package in R was used to visualize the distribution of DEPs.

2.10. Conservation and phylogenetic analysis

The functional domains of the candidate PLVAC proteins were predicted and analyzed using the Interpro and UniProt databases. Additionally, the biological function associated with these proteins and their interaction partners were investigated according to the STRING database. The corresponding protein sequences were used as queries to detect orthologues across eukaryotic organisms, including representative apicomplexan parasites, *Arabidopsis thaliana*, *Saccharomyces cerevisiae*, *Homo sapiens* and *Schistosoma japonicum*. These sequences were analyzed using both Blastp and the JackHAMMER engine. The top hit from the representative species in each taxon was chosen based on the ranking of the obtained *E*-value. Next, these selected orthologues were combined for conservation analysis, and were visualized with the ‘ComplexHeatmap’ package in R. Phylogenetic analyses were conducted in Tbtools software using the Mafft alignment algorithm with default parameters. The maximum Likelihood method was used to calculate the phylogenetic tree based on the trimmed amino acid sequences by trimAL software, and bootstrap values for 1000 iterations are indicated.

2.11. Plaque assay

For plaque assays, around 150 parasites were used to infect the fresh HFF monolayers in 6-well plates. The wells were supplemented either with 500 µM IAA (as an inducer) or 0.1 % ethanol, and incubated at 37 °C for seven days without disturbance. Afterward, the formed plaques were fixed with 70 % methanol for 15 min, followed by staining with crystal violet solution for 5 min. Following sequential washing and drying, the plaques were scanned, and the total number and size of the plaques were counted using Image J software.

2.12. Replication assay

Freshly collected parasites were grown on HFF monolayers in the 24-well plates with coverslips for 24 h, with or without IAA. After that, the monolayers were fixed and processed with IFA using rabbit anti-GAP45 polyclonal antibodies and corresponding secondary antibodies. At least 200 parasitophorous vacuoles (PVs) were counted blindly, and calculated across three biological replicates.

2.13. Invasion and egress assays

The intracellular parasites grown in ± IAA were collected by mechanically scraping the host cells, followed by resuspension in D5 medium and addition to 6-well plates with HFF monolayers on coverslips. The plates were centrifuged at 100 × g for 2 min to allow direct contact between the host cells and the parasites. After a water bath at 37 °C for 30 min, parasites and cell monolayers were fixed with cold 4 % paraformaldehyde for 10 min. The coverslips were incubated with monoclonal antibody against SAG1 (DG52, mouse derivative) without

permeabilization with Triton X-100, followed by a permeabilization step with Triton X-100 to allow entry of rabbit anti-GAP45 antibodies and corresponding secondary antibodies (anti-mouse and anti-rabbit). At least 15 fields per coverslip were visualized to count the intracellular or extracellular parasites using Nikon NI-E C2+ microscope.

For the egress assay, the parasites were grown on host cell monolayers for 36 h within \pm IAA for 24 h, prior to the egress assay, followed by stimulation with 3 μ M A23187 for 5 min at 37 °C and fixed using a cold 4 % paraformaldehyde solution for 10 min. The parasites were subjected to immunofluorescence assay (IFA) using mouse anti-GRA7 and rabbit anti-GAP45 as primary antibodies. The coverslips were mounted and visualized under Nikon NI-E C2+ microscope for quantification of vacuoles with egressed parasites or intracellular parasites. In the experiment, a total of 200 vacuoles per coverslip with three biological replicates were counted.

2.14. Parasite motility assay

Parental and AID lines were grown for 24 h, with or without auxin exposure for the final 6 h, before being purified for gliding assay. The parasites were placed in the 24-well plates with poly-lysine-coated coverslips, followed by incubation at 37 °C for 20 min and fixation with 4 % paraformaldehyde solution. The trajectory of parasite motility was visualized by the mouse anti-SAG1 and the corresponding secondary antibodies. The lengths of parasite gliding motility tracks retained on coverslips were measured, and at least 200 randomly selected parasites were scored in each replicate.

2.15. Microneme secretion

The parasite lines were cultured according to the experimental procedure described above. The parasites grown for 24 h were harvested and resuspended in a solution containing 1 μ g/mL A23187, followed by incubation at 37 °C for 10 min to simulate secretion of microneme proteins. Parasites were then centrifuged at 1500 rpm for 15 min, and the supernatant and precipitate were resolved by SDS-PAGE for western blot analysis. To assess microneme secretion in *T. gondii*, the mouse monoclonal antibody 6D10 (anti-MIC2) was used in the assay. In parallel, rabbit-anti-GRA7 antibodies were used to detect the constitutive secretion of the dense granule in the samples.

2.16. Fluo-4 AM calcium monitoring

Ca^{2+} release was measured using Fluo-4 AM, as described elsewhere [34]. Freshly lysed parasites were incubated with 250 nM Fluo-A4M (Beyotime, China) at 37 °C for 20 min, followed by centrifugation for 5 min. The parasites were washed twice with PBS, and then dispersed in 6-well plates containing poly-lysine-coated coverslips. After centrifugation at 100 g for 1 min, the parasites were treated with 1 μ g/mL A23187, followed by visualization under a fluorescence microscope from Olympus CO., Japan. The pixel intensities of the image were measured using ImageJ. The cytosolic Ca^{2+} concentration was measured by recording the changes in averaged values during the treatment of A23187.

2.17. Quantification of PLVAC size and Lysotracker staining

TgTEPSIN-AID and TgFYVE1-AID lines were served as the background strains to endogenously tag CPL gene at the C-terminus with 6 × HA epitopes. The distance of the widest dimension (for nonspherical compartments) of HA staining was used as the diameter of the PLVAC and was quantified using a Nikon confocal Ni-E C2⁺ microscope equipped with a DS-Ri2 microscope camera. Also, Purified parasites were resuspended in 1×10^8 parasites/mL in DMEM, and then incubated with 10 μ m Lysotracker Red for 30 min at 37 °C. The parasites were then washed in PBS and placed onto poly-lysine-coated coverslips.

2.18. GFP acquisition assay

The GFP acquisition assay was carried out as described in a previous study [35]. Briefly, the TIR1 and AID lines were maintained in GFP expressing HFF 1 monolayers, and treated with 10 μ M LHVS and IAA for 12 h. Purified parasites were placed on poly-lysine-coated coverslips, followed by permeabilization in PBS with 0.25 % Triton-X-100. The coverslips were then mounted in ProLong Gold Antifade Mountant containing DAPI for imaging under a Nikon Ni-E microscope. Parasites were categorized based on the presence of GFP foci, GFP diffusion, or absence of GFP, as depicted in Fig. 5F. Parasites were scored for each coverslip (at least 150 parasites). The proportion of parasites with GFP foci (GFP+) was calculated and expressed as a percentage of the total populations.

2.19. Mouse virulence assays

Female BALB/C mice (6-week-old) were randomly assigned to experimental groups, each consisting of five animals, and injected intraperitoneally (i.p.) with 100 *T. gondii* tachyzoites. These mice were administered with IAA daily by feeding and intraperitoneal injections, as described in our previous study [6]. In brief, the sterile water fed to the mice was adjusted to pH 8.0 and supplemented with 1 mg/mL IAA, 5 % sucrose (w/v), 3 mM NaOH, and flavored with 2 mg/mL TANG. The mice received daily i.p. injections of 0.2 mL of a sterile solution adjusted to pH 7.8 containing 15 mg/mL IAA and 1 M NaOH. Body weight and survival status were monitored daily for up to 20 days.

2.20. Transmission electron microscopy (TEM)

Parasites were harvested and fixed overnight at 4 °C in a solution containing 2 % paraformaldehyde and 3 % glutaraldehyde. After washing with PBS, the samples were exposed to 1 % osmium tetroxide at ambient temperature for 2 h, followed by dehydration through a graded series of ethanol and acetone concentrations, then incubation in Spurr's resin for 1 h. The samples were then embedded and prepared for ultrathin sections with 60–80 nm thickness slides with a Leica EM UC7 ultramicrotome. The sections were placed on single-hole grids coated using a Formvar membrane, followed by staining with lead citrate and 2 % uranyl acetate, and were finally visualized with a Hitachi HY7800 transmission electron microscope.

2.21. Transcriptomic sequencing and qRT-PCR assay

After 12 h of post-infection in cell monolayers, parasites were harvested by syringed lysis, filtered, and resuspended in pre-chilled Trizol (Invitrogen). After purification of total RNA, the quantity and integrity of RNA were assessed, and used to generate paired-end (2 \times 150 bp) cDNA libraries. The samples were then sequenced using Illumina HiSeq2500 platform of Gene Denovo Biotechnology Co. (Guangzhou, China). Raw data were trimmed to remove low-quality reads, adapter sequences, and other unknown bases ('N' base) using fastp (version 0.18.0). Clean reads were mapped to the *Toxoplasma gondii* genome (ToxoDB release 65. <http://toxodb.org/toto/app>) using Histat2 (version 2.1.0), and gene expression levels were normalized using the TPM method. Differential gene expression was analyzed using the DESeq2 package in R, with genes featuring a *P* value below 0.05 and absolute fold change above 1.5 deemed significantly differentially expressed. Further downstream analysis, including GO and KEGG enrichment, was performed using the 'ClusterProfiler' package [43].

The qPCR assay was carried out on a StepOneTM Real-Time PCR System. The qPCR volumes and amplification procedure followed a standard protocol that uses 100 to 500 ng of mRNA as templates. The corresponding primers used for the reactions are listed in Table S1c. The cycle threshold (CT) values per gene were employed in the $\Delta\Delta\text{CT}$ formula to determine their relative expression level, which were then analyzed

with GraphPad Prism 8. TgActin served as the housekeeping gene for normalization purposes.

2.22. In vitro differentiation

Bradyzoite differentiation was assessed by culturing parasites in the alkaline RPMI-HEPES medium (pH 8.2) at 37 °C without CO₂. The parasites were grown in an environment with or without IAA for 72 and 96 h. Next, the samples at the different time points were collected for IFA processes using primary antibodies against IMC1, and were then incubated with FITC-conjugated DBL to label the parasite cyst wall. The stage-specific images of cyst development in parasites were visualized and the percentage of DBL-positive or negative PVs were scored with >200 vacuoles counted per replicate. Each experiment was independently performed in triplicate. The relative expression levels of BAG1 were also quantified using the qRT-PCR method mentioned above.

2.23. Statistical analysis

All statistical analyses in the study were conducted using GraphPad Prism software (version 8.0.2.). Multiple category comparisons were analyzed by two-way analysis of variance (ANOVA) with Tukey's multiple comparisons. Two groups of independent data were tested using the unpaired *t*-test method or Mann-Whitney test, depending on whether the data satisfied a normal distribution. Statistical significance was defined as *P* < 0.05. All associated statistical method details including trials (N), replicates (n) and statistical tests used are described in corresponding figure legends.

3. Results

3.1. Construction of TurboID-CPL and CRT-TurboID parasite lines

Although the PLVAC has been explored for 14 years since its discovery, several predicted functions, such as vesicle transport and fusion,

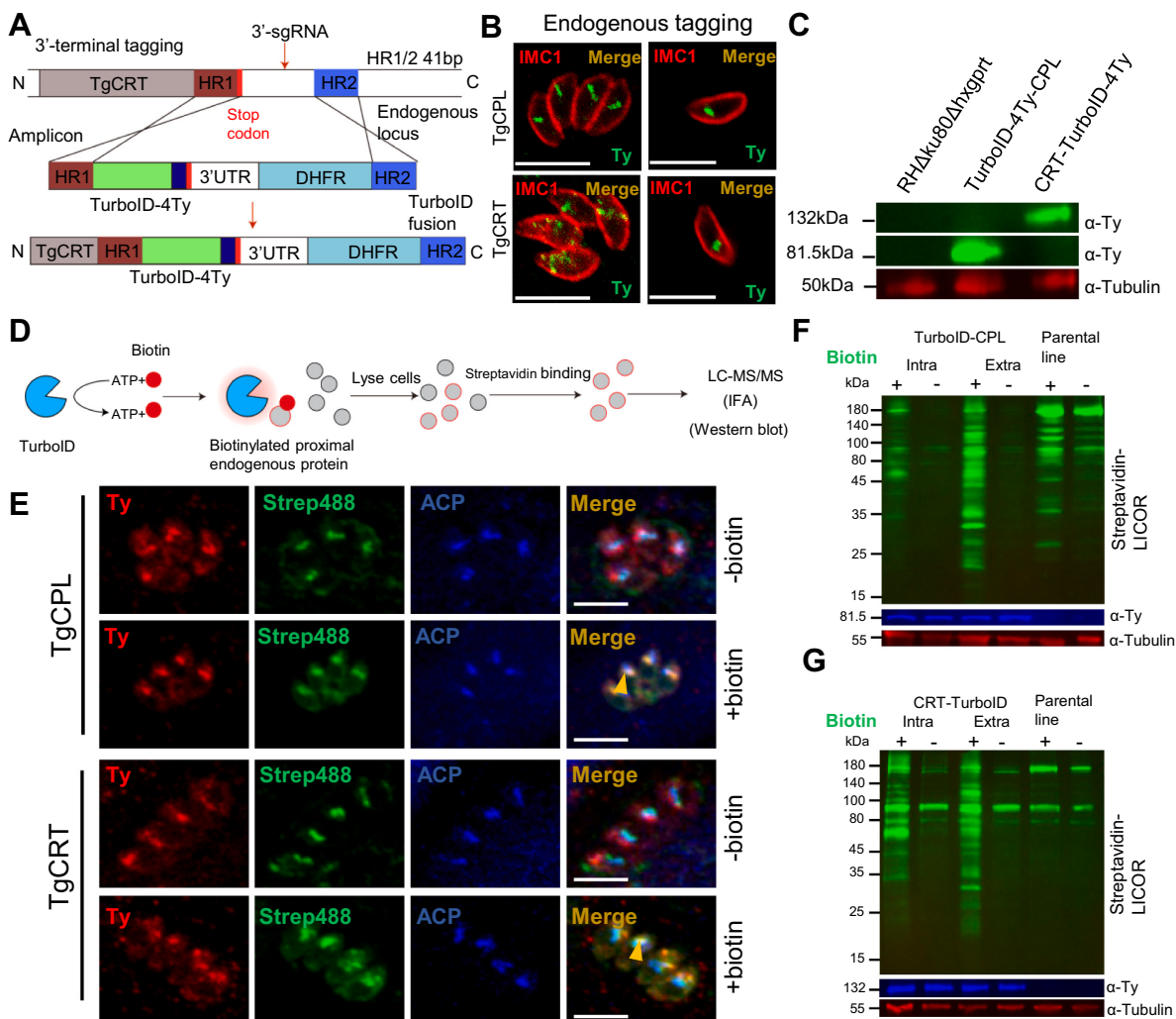


Fig. 1. Construction of CPL and CRT-TurboID lines in *T. gondii*. (A) Schematic diagram depicting the CRISPR-mediated C-terminal TurboID-4Ty tagging strategy at the endogenous locus of the 3'-terminus of TgCRT in the background strain RHΔku80Δhxgprt. For the endogenous tagging of CPL, TurboID-4Ty was inserted in front of the start codon of TgCPL using a similar tagging approach. (B) Indirect fluorescence assay (IFA) of the TurboID parasite lines showing the localization using antibodies against Ty (green) and IMC1 (red). (C) Western blot showing the expression of integrated TurboID-4Ty fragment fused at the target proteins. Tubulin served as the loading control. (D) Schematic of the TurboID proximal proteomic approach used in our study. (E) Parasites collected from intracellular conditions were grown in 500 μM D-biotin for 90 min, and biotinylated proteins (green) were detected using streptavidin reagents on IFA. ACP was used as a control to label the biotinylated proteins in the apicoplast, while antibodies of Ty epitopes and tubulin show the TurboID fusions and the loading control, respectively. The arrowheads indicate streptavidin fluorescence signals on the PLVAC. (F-G) Western blots also showing the additional bands compared to the parental lines in the intracellular (intra) and extracellular (extra) parasites. TgTubulin was used as a control. Bar = 5 μM. Two-three independent experiments were performed with similar outcomes.

membrane transport, formation and maintenance of the PLVAC, along with its low pH, remain unanswered. To further investigate the proteomics and identify proteins responsible for the predicted functions of the PLVAC in *T. gondii*, we employed the proximity biotin labeling enzyme TurboID by fusing it with markers (TgCPL and TgCRT) of the PLVAC. In the study, the N-terminus of TgCPL and the C-terminus of TgCRT were fused with TurboID-4Ty at the endogenous locus of the respective terminus using the CRISPR tagging approach, as illustrated in Fig. 1A and in our previous studies [6,36]. We corroborated the successful fusion of the two TurboID lines in the parasite lines by using diagnostic PCR and immuno-fluorescent assay (IFA), as demonstrated by the correct subcellular localization and single band of proteins (Fig. 1B and C). To assess the biotin ligase activity of TurboID and identify PLVAC-associated proteomics, the parasites were incubated with biotin, followed by harvesting parasites for streptavidin staining in IFA or western blots and subsequent mass-spectrometry procedure (Fig. 1D). Firstly, for the IFA diagnostic assays, we naturally observed the co-localization between apicoplast marker ACP and streptavidin signal under the absence of biotin. In contrast, after the addition of biotin, the additional signal spots were largely co-localized with the Ty epitope (Fig. 1E). Furthermore, additional bands on western blots were also found in both extracellular and intracellular parasites of the two TurboID fusion lines (Fig. 1F and G). These results suggested that the TurboID approach successfully labels proximal proteins associated with the PLVAC in the parasite.

3.2. Identification of novel PLVAC proteins in the *T. gondii*

To mine additional candidate proteins, mass-spectrometry analysis was conducted from the purified samples obtained from the parental line RHΔku80Δhxgprt (denoted as CK in the assay) and the two TurboID fusion lines (denoted as CPL and CRT). The obtained mass spectrometry datasets ($N = 2$ for each sample, with intracellular and extracellular parasites of each line) containing both qualitative and quantitative results were exported into an Excel spreadsheet (Table S2A), and the combined datasets (for the intracellular and extracellular parasites) were analyzed using R software to identify the differentially expressed proteins (DEPs), by comparing datasets from the CPL and CRT to the CK, respectively. The volcano plots showed that the proteomic analyses identified the baits TgCPL and TgCRT in samples of the TurboID fusions among the top candidates with high fold-changes (Fig. 2A and B), as expected for the fusion proteins, suggesting the robustness of the proximity biotin labeling approach in the study. We noticed that known PLVAC proteins, TgASP1 and TgZnT, were identified as the DEPs in the fold-change analysis. To screen the candidates, we set the basic criteria for the candidates at the foldchange >1.5 , yielding 259 and 106 DEP candidates in CPL vs. CK and CRT vs. CK, respectively. Notably, this analysis found 74 shared candidates between the CPL and CRT groups (Fig. 2C). Based on the shared candidates, we further analyzed, tagged, and experimentally screened the targets using literature mining as well as genetic and cellular approaches, as illustrated in Fig. 2D.

We then obtained a list of 41 candidates (here named as VAP1–41) for screening of the PLVAC proteins by genetic tagging and generation of parasite lines. We successfully generated 41 lines at the C-terminus of the candidates. Indirect fluorescence assay (IFA) in the genetically-modified lines showed that 14 VAP-6Ty fusions out of 41 candidates were localized to a concentrated foci inside the parasites, resembling the position of the PLVAC (Fig. S1A). Other candidate lines displayed some characteristic structures for the candidate proteins, which include the cytosolic vesicles (VAP8, VAP9, VAP37), the endoplasmic reticulum (VAP5, VAP28), the cell nucleus (VAP2, VAP3, VAP6 and VA19), the residual end (VAP13), or other structures (e.g. VAP35) (Fig. S1B). To clarify the precise localization of the candidates localized to the concentrated foci inside the parasite, confocal imaging was further performed to verify the potential co-localization of the candidates with the PLVAC marker CPL, which showed that 9 out of the 14 candidates

present almost perfectly co-localized with CPL with a Pearson correlation coefficient (PCC) ≥ 0.9 (Fig. 2E).

3.3. *TgTEPSIN* and *TgFYVE1* are predicted to be involved in vesicle-mediated transport and conserved in eukaryotes

The functional domains were determined by searching the corresponding amino acid sequences on the Interpro website. The analysis showed that many of the proteins contain specific domains, which include Magnesium transporter MRS2-like (VAP30), PX (VAP24, termed TgPX2), organic solute transporter (VAP12), FYVE zinc finger (VAP27, termed TgFYVE1), TM9SF (VAP32), Glycerophosphodiester phosphodiesterase (VAP40) and ENTH Domain (VAP23, termed TgTEPSIN) (Fig. 3A). We further utilized the STRING database to predict their potential function and their interaction proteins encoded in the *T. gondii* genome. Notably, the interaction network suggested that TgTEPSIN and TgFYVE1 were clearly enriched in the Gene Ontology (GO) term “vesicle-mediated transport”, while most of the proteins are classified into the GO term “predicted transporters and unknown proteins” (Fig. 3B). These predictions with novel proteins identified in this study match with the above predicted functions for the PLVAC, suggesting that this work could answer some of the key questions raised above.

We further analyzed the conservation of the novel proteins in the representative species of the subphylum Apicomplexa, *A. thaliana*, *S. cerevisiae*, *H. sapiens* and *S. japonicum*. The Hidden Markov Model (HMM) searching identified the best hits with the cutoff *E*-value of 1×10^{-7} in these species, with which the conservation was visualized using the Complex Heatmap package in R. The analysis showed the high conservation of four proteins (TgTEPSIN, TgFYVE1, VAP30 and 32) in all available apicomplexan species including *P. falciparum* (Fig. 3C), yet other novel proteins were unidentifiable in the species, suggesting less conservation of the novel proteins identified in this study compared to those of the previously known PLVAC proteins. Among the four proteins, we noted that no associated reports for the homologs of the other three proteins except TgTEPSIN being found in *Plasmodium* species. Specifically, the homology of TgTEPSIN in *P. falciparum* was identified as a significant marker associated with artemisinin resistance in a genome-wide study. This discovery further motivated our interest in exploring the evolutionary relationships and conserved sites of this protein across different species. To investigate this, we constructed a phylogenetic tree based on the homologs identified in several representative species and revealed other apicomplexan parasites except piroplasmida (including Theileria and Babesia sp.) exhibit close phylogenetic relationships with both mammals and plants (Fig. S3A). Meanwhile, multiple Sequence alignment of TgTEPSIN targeting the ENTH domain clearly showed that residues have varying levels of similarity, highlighting the potential functional significance of this domain (Fig. S3B). Accordingly, the detailed information including accession number and *E*-value for these homologous proteins were listed in Table S3.

3.4. *TgTEPSIN* is important for the lytic cycle of *T. gondii*

The GO term analysis showed possible roles of the novel proteins in the PLVAC. We then attempted to examine the roles by conditional down-regulation of these proteins using a plant auxin-inducible degron (AID) system. To do that, we generated the AID fusion lines for all the genes encoding these novel proteins in a CRISPR-tagging approach, and the diagnostic PCR was performed for integration of the AID fragment at the 3 termini of the genes, which showed the correct sizes of PCR products as expected (Fig. S2A). Prior to testing growth defects by plaque assay, we examined the parasite lines by IFA to verify the capability of protein down-regulation by the AID system, which showed that the AID fusions in the lines were undiscernible after 12 h of induction by auxin (Fig. S2B). Collectively, the novel proteins fused with the AID tag were successfully regulated by the AID system by addition of auxin.

T. gondii undergoes a lytic cycle, which includes parasite invasion,

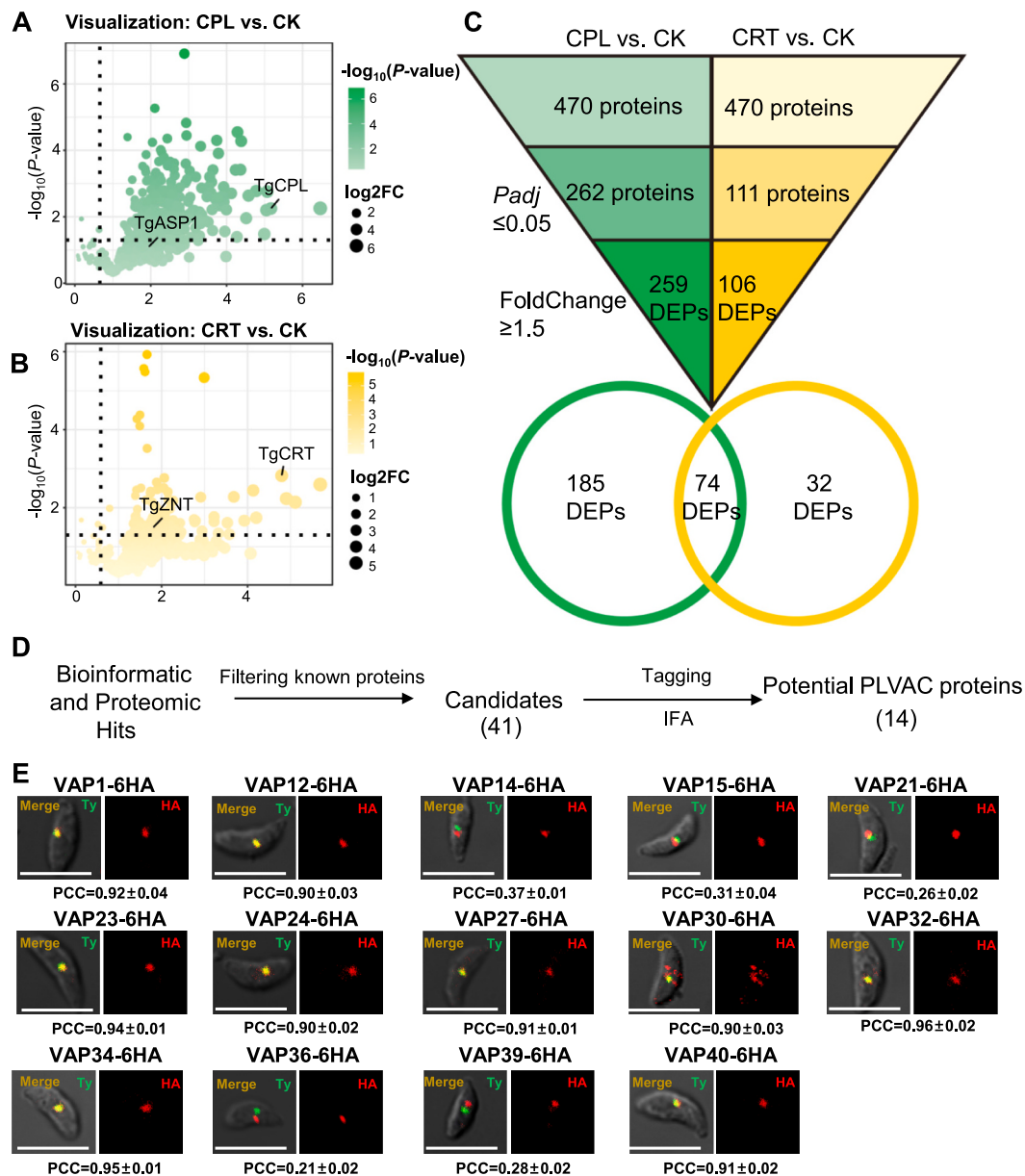


Fig. 2. Discovery of novel PLVAC proteins from the TurboID proximal proteomes in *T. gondii*. Volcano plots showing the TgCPL vs. RH (A) and TgCRT vs. RH (B) comparisons. The known PLVAC proteins, such as TgCPL, TgASP1, TgCRT and TgZnT, were pointed out in the plots. Dashed lines (vertical and horizontal) indicate the fold change at a level of 1.5 and with $P = 0.05$. (C) The differentially expressed proteins (DEPs) were screened with $P \leq 0.05$ and absolute fold change ≥ 1.5 for the two mass-spectrometry datasets. The common DEPs identified in the comparison were presented by a Venn diagram. (D) The workflow was utilized to identify PLVAC proteins (see details in Table S2a and b) in the study. (E) Co-localization analysis of the candidates VAPs and the PLVAC marker CPL. The VAPs were endogenously tagged with 6HA epitopes in the background line of CPL-6Ty, followed by IFA analysis of extracellular parasites using anti-Ty (green) and anti-HA (red) antibodies. The Pearson correlation coefficient (PCC) values were analyzed for 50 individual parasites, and shown with mean \pm SD. Bar = 5 μ m.

replication and egress, thus progressively lysing nearby host cells and producing plaque areas in host monolayers (Fig. 4A). We then examined the lysing activity of the parasite lines by growing the lines in host cell monolayers under the presence or absence of auxin for 7 days. The analysis showed that the parasite lines grew normally in the absence of auxin, and many of the lines, such as TgPX2, VAP30 and 32, did not display obvious defects of plaque formation in the presence of auxin (Fig. 4B). In contrast, the lines of TgTEPSIN and VAP34, had clear defects of plaque formation when grown in auxin, compared to the parental line TIR1 in auxin (Fig. 4B). We then further analyzed the essentiality of the novel proteins by scoring numbers and sizes of plaques formed by the parasite lines from three independent experiments with triplicates. Indeed, we confirmed loss of plaque formation in the TgTEPSIN-AID fusion in auxin, and significant reduction of plaque

numbers and sizes in the VAP34-AID parasite line (Fig. 4C and D). Based on the assay of plaque formation, we further conducted a replication assay for the AID fusion lines to test if depletion of the proteins was able to affect the parasite replication inside the host cells. The counting and scoring results demonstrated that the percentages of parasites per vacuoles at the 24-h growth time point were significantly changed in the lines of TgTEPSIN-AID and VAP34-AID lines (Fig. 4E), supporting the strong defects in TgTEPSIN-AID and VAP34-AID. To gain an overview of the PLVAC components in protein essentiality, we compiled a table that summarizes the CRISPR fitness scores and plaque formation results (Fig. 4F). The results clearly supported that TgTEPSIN is as important for parasite growth as the previously published TgVHA1 protein.

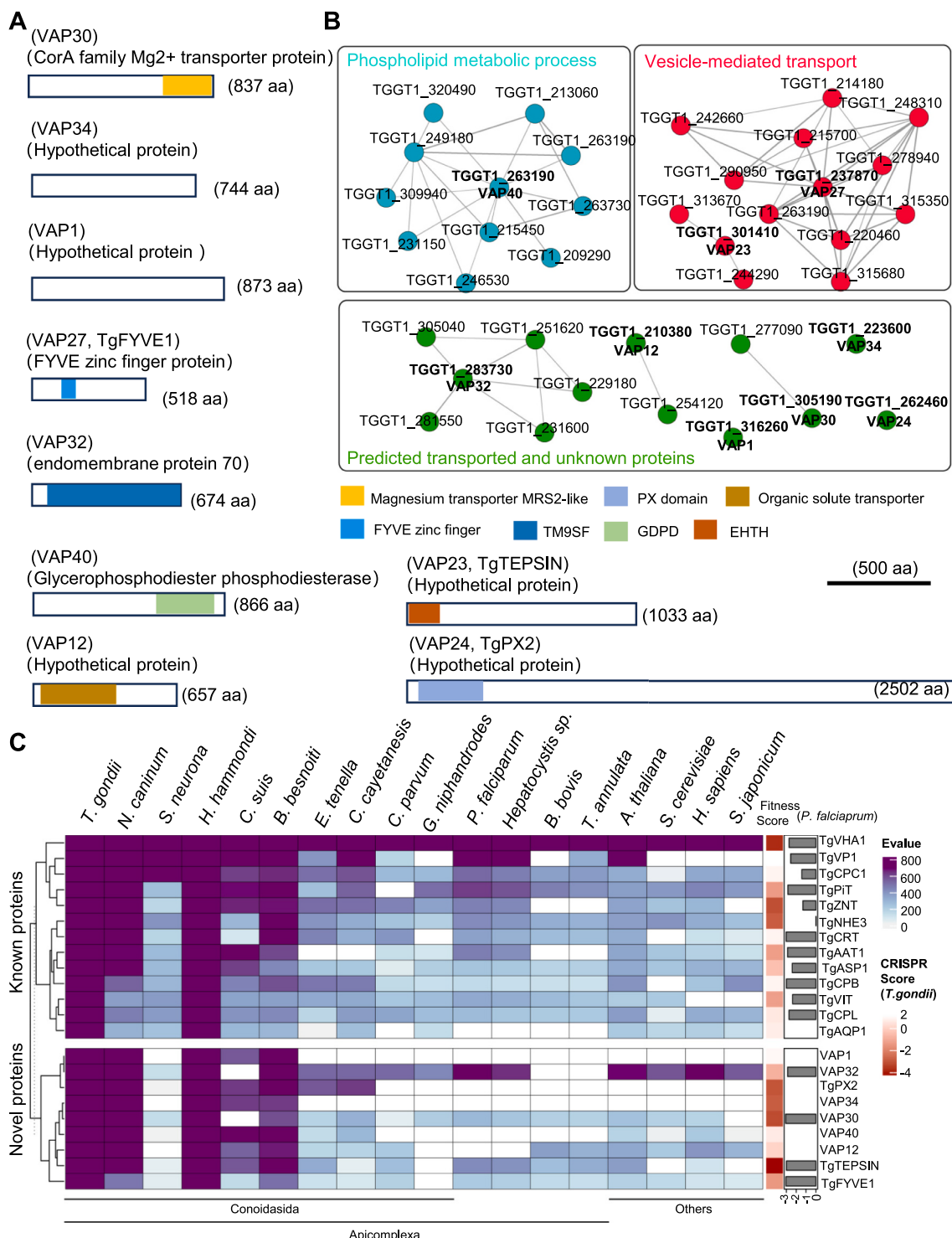
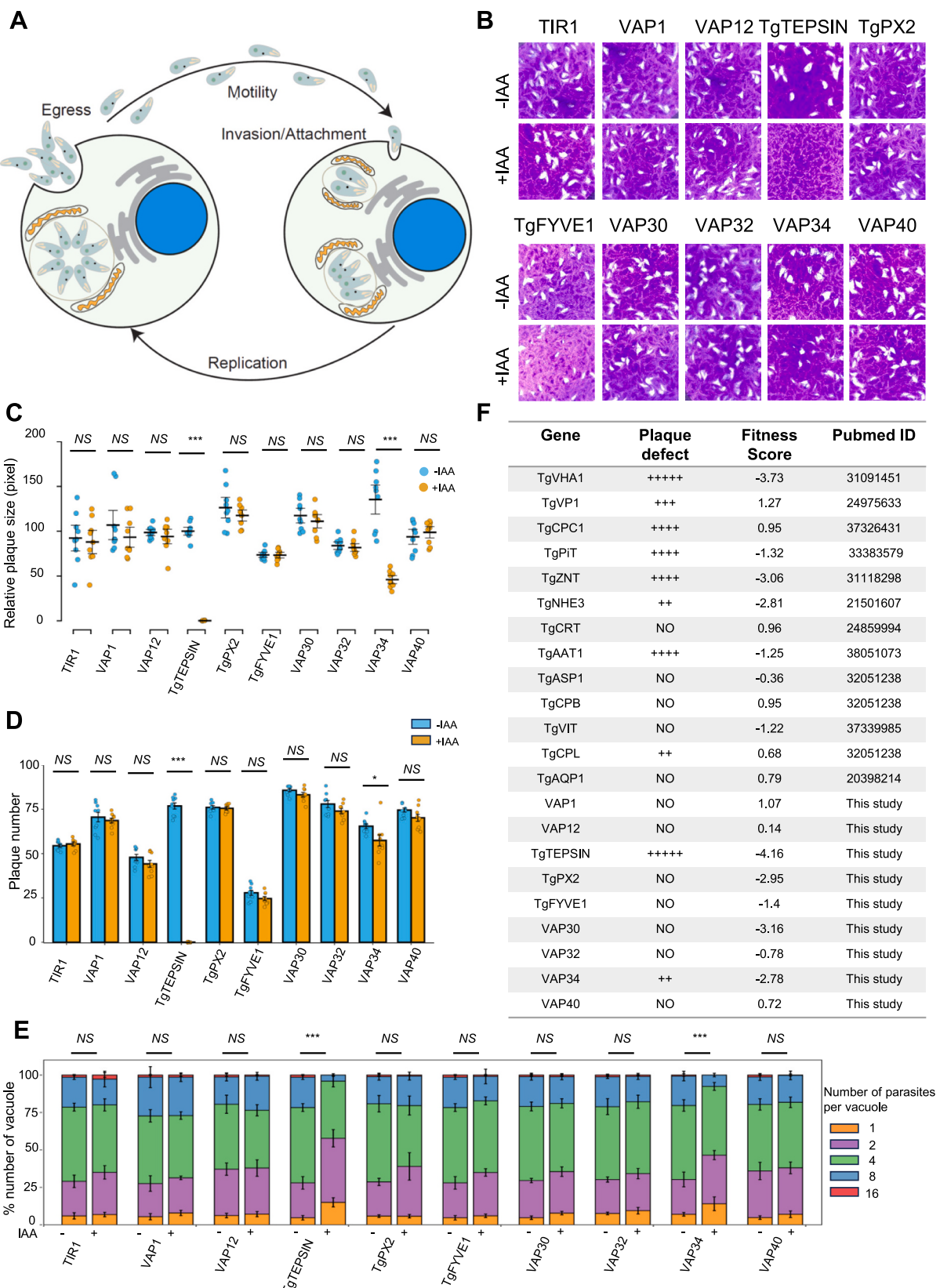


Fig. 3. Bioinformatic analysis of newly identified PLVAC proteins in *T. gondii*. (A) The schematic plot depicts the domain sites of the 9 PLVAC proteins by the InterPro website (<https://www.ebi.ac.uk/interpro/>). Scale = 500 aa. (B) The STRING database (<https://version-11-5.string-db.org/>) was used to perform the functional prediction for the newly identified proteins. (C) The heatmap of conservation for best hits of the 9 PLVAC proteins identified in this study and 13 known PLVAC proteins identified previously. On the right of heatmap, the fitness scores of *T. gondii* proteins were displayed in red for *T. gondii* (ToxoDB, <https://toxodb.org/>) and grey bar plot for the homologs identified in the *P. falciparum* genome (PlasmoDB, <https://plasmodb.org/>). UPGMA method was used to cluster the tree dendrogram across proteins based on their E-value.

3.5. Depletion of TgTEPSIN results in defects in parasite invasion, secretion of microneme proteins and GFP transport

In the above GO term analysis, TgEHTHD2 and TgFYVE1 were predicted to have a role in “vesicle-mediated transport” and were conserved

in most eukaryotes. Based on these features, we then focused on the phenotypic dissection of these two proteins, specifically TgTEPSIN. Before analyzing the phenotypes, we performed western blots to check the kinetics of protein depletion by the AID system, from which we observed that the proteins were efficiently down-regulated by auxin



(caption on next page)

Fig. 4. Plaque formation and replication assay of the knockdown lines. (A) The diagram shows the lytic cycle that includes three basic steps: parasite invasion, parasite replication and egress from host cells. (B) Plaque assays of clones grown in \pm IAA for 7 days. Parasites (150 parasites per well) were cultured on 6-well plates for 7 days, followed by fixation and staining with crystal violet. Plaque sizes (C) and numbers (D) were measured by ImageJ software. (E) Replication assay of the TIR1 and AID lines grown in \pm IAA for 24 h, followed by IFA analysis of parasites by antibodies against GAP45. Vacuoles with different numbers (1, 2, 4, 8 and 16) were counted (≥ 200 vacuoles for each replicate); (F) The table shows the fitness scores and plaque defects of known and newly identified PLVAC proteins. The fitness scores were retrieved from the CRISPR/CAS9 library screen [37] that has been uploaded to the TOXOdb (<https://toxodb.org/toxo/app>), while the symbol with plus (from + to +++) indicates the severity of plaque defects reported from previous studies as indicated by the PMID numbers. The plus (+) symbols denote the degrees of defect from the highest (an essential feature) to the lowest (with NO or +) for the proteins listed. Three independent experiments with triplicates were performed and data from plaque size and numbers are analyzed by the two-tailed, unpaired t-test and shown as mean \pm SD. The obtained data ($N = 3$ independent experiments; $n = 3$ replicates) from the replication assays were presented as a mean \pm SD with two-way analysis of variance (ANOVA) with Tukey's multiple comparison test. (NS, not significant; * $P < 0.05$; ** $P < 0.001$; *** $P < 0.0001$). Bar = 5 μ M.

even in the induction time of 1 h (Fig. S2C). Due to the moderate defect in the parasite replication at the induction time of 24 h (1, 2, 4 and 8 parasites per vacuole still appear upon depletion of the TgTEPSIN), we suspected that the parasites depleted of TgTEPSIN harbor other defects related to parasite invasion or parasite egress in the lytic cycle. We then performed an invasion assay by a pulse invasion of the parasites for 30 min, and by staining extracellular parasites with parasite surface protein SAG1 prior to permeabilization of the parasites, followed by staining of intracellular parasites with IMC1. When TgTEPSIN protein was degraded in the presence of auxin for 12 h, TgTEPSIN-AID strain showed a significant decrease in cell attachment compared with that of the parental line (Fig. 5A). Correspondingly, in the invasion assay, the parasites of TgTEPSIN-AID grown in auxin for 12 h further decreased to about 15 % of the parasites without auxin (Fig. 5A), suggesting a strong defect in invasion capability in parasites depleted of TgTEPSIN. To examine if the proteins are involved in another event of the parasite lytic cycle – parasite egress, we stimulated the parasites to egress from the host cells by incubation with 3 μ M A23187 for 5 min. Notably, the parasite egress was strongly reduced in the TgTEPSIN-AID line induced in auxin for 12 h, compared to the parental line and parasites without auxin (Fig. 5B).

We next wondered if the proteins can regulate the parasite motility, likely by being involved in protein sorting or maturation of the apical micronemes. To do the assay, purified parasites are allowed to incubate on coverslips for 10 min, followed by staining with antibodies against the extracellular protein SAG1. The SAG1 staining indicates residual trails retained during parasite gliding, the length of which could represent capability of parasite motility, as demonstrated in Fig. 5C. In the TgTEPSIN-AID grown in auxin, we observed significantly reduced length of parasite gliding trails, compared to that of the parental line and the parasite without auxin (Fig. 5D). Notably, in the TgFYVE1-AID, we did not observe any significant defects in the above measurements, thus supporting the reliability of the assays.

Furthermore, the microneme secretion and nutrient uptake from host cells were also examined in the study. First, we observed the western blots showed that the MIC2 intensity in the supernatant were significantly reduced in the parasites grown in auxin (Fig. 5E), as indicated by the quantification of three independent experiments using the constitutively secreted GRA7 protein as control (Fig. 5F). We therefore concluded that the reduced secretion of microneme proteins is likely to be caused by reduced protein level in TgTEPSIN depleted parasites. For the GFP transport assay, the markedly decreased GFP accumulation ratio also further reinforces the role of TgTEPSIN in the nutrient uptake from host cell (Fig. 5G and H).

To further investigate the involvement of the two proteins in tachyzoite virulence, an intraperitoneal infection was employed in which mice were inoculated with 200 tachyzoites from either the TIR1 parental strain and the two AID-modified strains. The mice received daily oral and intraperitoneal administrations of either a control vehicle or auxin. The survival analysis indicated that all mice infected with either the TIR1 parental or TgFYVE1-AID strains, and subsequently treated with IAA, succumbed by days 8–12. In contrast, TgTEPSIN-AID parasites administered IAA keep all mice survive throughout the study period (Fig. 5I). Further observations of body weight trends revealed

that mice infected with the TgTEPSIN-AID line and receiving auxin maintained steady weight gain by day 3, while those infected with the other strains experienced significant weight loss by days 3–4 (Fig. 5J). Collectively, these findings highlight TgTEPSIN as a critical factor for parasite replication and virulence in vivo, underscoring its potential role in the pathogenicity of tachyzoites.

3.6. Depletion of TgTEPSIN caused diffusion of the PLVAC in the parasite

Next, we endogenously tagged CPL gene at the C-terminus with 6 \times HA based on two AID lines as the background strain using a CRISPR/Cas9 approach. Through IFAs analyses, the similar results for the vesicles distributed through the cell were observed in extracellular and intracellular TgTEPSIN-AID+IAA parasites (Fig. 6A). And we found a significant difference in the PLVAC diameters (or the widest dimension) from TgTEPSIN-AID +IAA parasites as compared with the controls (Fig. 6B), further supporting the more important role of TgTEPSIN than TgFYVE1 in the biogenesis and dynamics of PLVAC. Lysotracker Red is a lysosomal red fluorescent probe that is permeable to cell membranes and stains specific lysosomal compartment in living cells. When we loaded TgTEPSIN and TgFYVE1-AID lines with 10 μ M Lysotracker under the IAA treatment for 12 h, the dilated areas instead of the single vacuole labeled in the apical position of TgTEPSIN-deficient parasites showing the fragmentation of the PLVAC, whereas no differences were found in the TgFYVE1-deficient parasites (Fig. 6C). Given that, we next looked at the changes in distribution of several important *T. gondii* organelle markers following depletion of TgTEPSIN by addition of IAA. Notably, all the staining of makers was localized to the expected locations in TgTEPSIN-AID lines with IAA (Fig. S3).

To further confirm the results obtained from IFAs, we then examined the ultrastructural characteristics in extracellular TgTEPSIN-depleted parasites. In non-induced parasites showing intact cellular architecture, we observed the presence of the well-organized and neatly distributed secretory organelles including rhoptry and microneme, and the prominent feature PLVAC (Fig. 6D, panel i). In addition, we also mainly inspected the content and shape of PLVAC compartment in extracellular TgTEPSIN-depleted parasites. PLVAC structure indeed displayed varying degrees of alterations and distortions. Some representative images of EM were selected and clearly indicated that PLVAC can fragment into a few or multiple membranous structures and vesicles in the top of parasites (Fig. 6D, panel ii) or enlarge content of the compartment (Fig. 6D, panel iii). Of interest, in some fields of view, vacuolization was observed inside the normally shaped parasites, seemingly occupying the entire cell, which was not seen in the control group (Fig. 6D, panel iv). Moreover, the percentage of each abnormal phenotypes was calculated from 100 parasites (Fig. 6E), suggesting the loss of TgTEPSIN results in the alteration of PLVAC morphology and content.

3.7. Depletion of TgTEPSIN affects the calcium signaling pathway

To further detect the global alterations of transcriptome profiles related to the conditional knockdown of TgTEPSIN, we performed RNA-Seq analysis on TgTEPSIN AID fusion lines and parental TIR1 lines

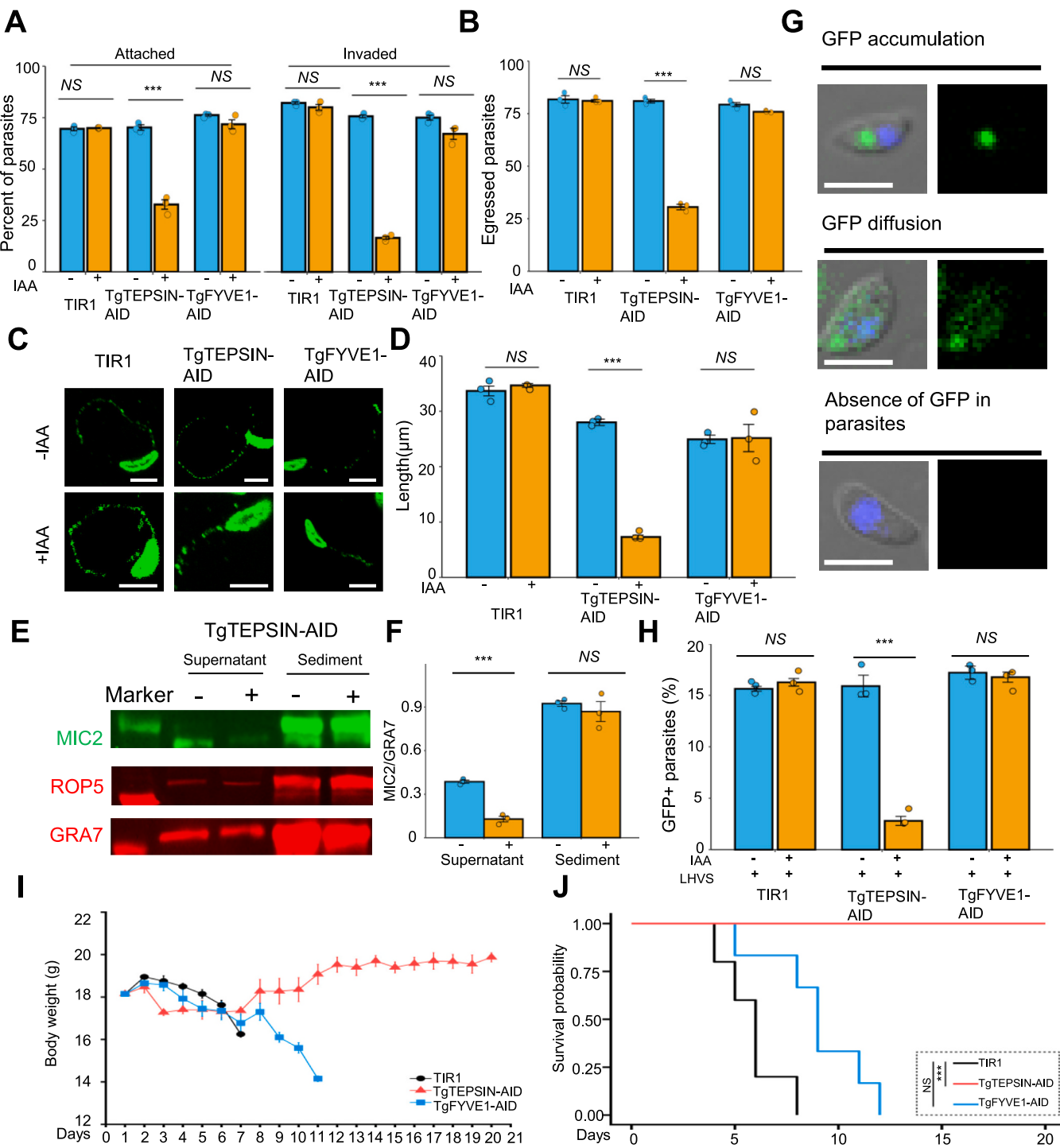


Fig. 5. Phenotypic analysis of the parasites depleted with TgTEPSIN. (A-C) Analysis of parasite motility, invasion and egress of the parasite depleted with TgTEPSIN. The parental and AID parasite lines were grown in \pm IAA for 12 h, followed by harvesting of the parasites by mechanically forced egress and incubation of the parasites on host cells monolayers to allow parasite invasion (A) or incubation of the parasites on coverslips coated with poly-lysine to allow parasite gliding (B-C). The parasites were then analyzed by IFA using SAG1 antibodies without a Triton-X100 permeabilization step, and the samples for the invasion assay were further stained by GAP45 antibodies after permeabilization. (D) The egress assay of the parasites. The parasites grown for 36 h but induced in \pm IAA for 12 h were stimulated with 3 μ M A23187 for 5 min, followed by IFA analysis using antibodies against GRA7 and GAP45. (E) Depletion of TgTEPSIN resulted in a defect in the normal secretion of MIC2. The parasites grown as described in E were harvested for stimulation of extracellular parasite to secrete MIC2 by 1 μ M A23187, followed by SDS-PAGE and western blot of the supernatant and pellet. (F) Quantification of MIC2 secretion by Image J (ratio of MIC2/GRA7). Data were compiled from three independent experiments. (G, H) GFP transport was significantly affected by the depletion of TgTEPSIN-AID. The parasites were grown in host cell monolayers supplemented with 10 μ M LHSV for 12 h, followed by purification of the parasites for scoring of parasites containing a concentrated GFP focus, GFP diffusion, or absence of GFP signal. Examples of those parasites and the quantification outcomes were shown in F and G, respectively. (I-J) The acute virulence of TgTEPSIN and TgFYVE1-deficient parasites was evaluated in a murine model via intraperitoneal infection. The body weight (I) and mortality (J) of the mice were monitored and recorded for 20 days. Data ($N = 3$ independent experiments; $n = 3$ replicates) from the above assays were analyzed by the two tailed, unpaired t -test and shown as mean \pm SD indicated by the same colour dots. (NS, not significant; * $P < 0.05$; ** $P < 0.001$; *** $P < 0.0001$).

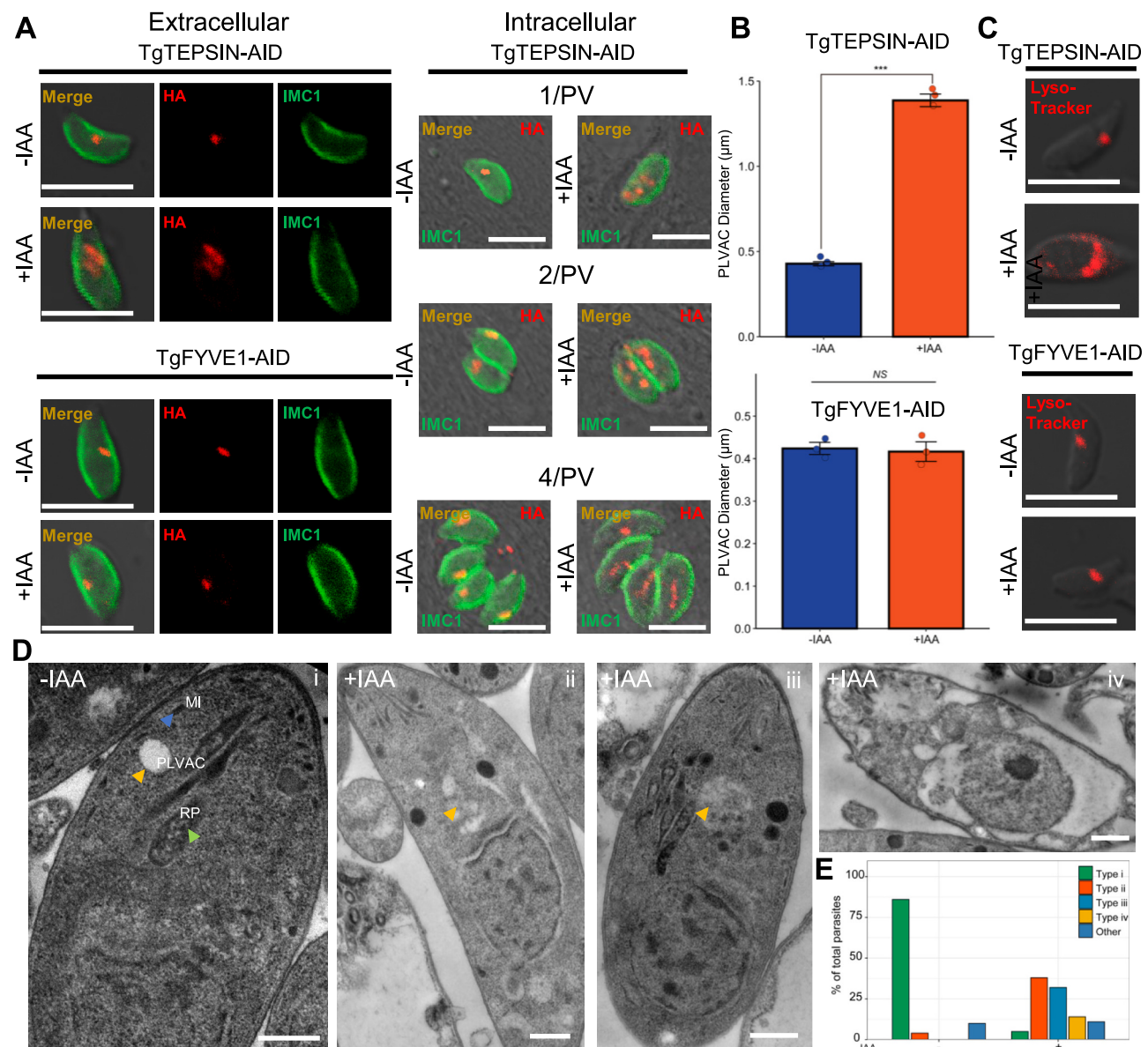


Fig. 6. Depletion of TgTEPSIN resulted in diffusion of the PLVAC. (A-B) Diffusion of the PLVAC marker CPL was evident in the parasites depleted with TgTEPSIN and TgFYVE1. The two AID lines endogenously tagged CPL gene were grown for 36 h but in \pm IAA for 12 h, followed by harvesting of the parasites for IFA using anti-HA antibodies (red) and IMC1 (served as the control, green). The parasites in one, two and four intracellular parasites per vacuole were analyzed in parallel. (B) Measurement the PLVAC diameter in parasites depleted of TgTEPSIN. The diameter was measured for the parasites imaged in a Nikon confocal Ni-E C^{2+} microscope equipped with a DS-Ri2 microscope camera, and at least 50 parasites were measured in each replicate. For nonspherical PLVACs, we measured the widest dimension. Data ($N = 3$ independent experiments; $n = 3$ replicates) from the above assays are analyzed using unpaired two-tailed Student's *t*-test. (NS, not significant; * $P < 0.05$; ** $P < 0.001$; *** $P < 0.0001$). (C) LysoTracker staining of the parasites depleted of TgTEPSIN. The parasites were grown for 36 h but in \pm IAA for 12 h, followed by incubation of the parasites with LysoTracker red for 30 min at 37 °C in PBS. (D) Transmission Electron Microscopy (TEM) of extracellular TgTEPSIN-AID parasites. A TEM image of control sample (panel i) showing morphologically normal structure including apical micronemes (MI; blue arrowheads), rhoptries (RP; green arrowheads) and PLVAC (yellow arrowheads). Representative EM of PLVAC (yellow arrows) from the TgTEPSIN-AID parasites treated with IAA for 12 h, characterized by multi-vacuole compartments or dispersed multivesicular structures in the apical end (panel ii), enlarged compartment (panel iii) and vacuolization throughout the cell (panel iv); Bars, 500 nm. (E) The percentage for all observed phenotypes were counted from 100 TgTEPSIN-AID parasites with and without IAA. The parasites with severely irregular morphology were classified as "others".

grown in auxin for 12 h. First, Principal component analysis (PCA) revealed 23 % of the total variance and clearly separated all six samples into two categories corresponding to their origins, which provides a clear indicator for subsequent analysis (Fig. 7A). Using 'DESeq2' package, the results identified a total of 503 significant differentially expressed genes (DEGs), with 333 that are up-regulated and 170 genes down-regulated in the experimental group (TgTEPSIN-AID) versus the control TIR1 (Fig. 7B). Among the list of top five down-regulated DEGs, TgCPL was significantly reduced 6-fold lower transcript levels due to the

depletion of TgTEPSIN, as evidenced by the q-PCR analysis (Fig. 7C). In addition, GO enrichment analysis showed that the lipid and fatty acid catabolic processes, V-type ATPase complex component and microtubule binding were markedly affected (Fig. 7D). Meanwhile, KEGG enrichment further demonstrated the depletion of TgTEPSIN involved in cAMP, cGMP-PKG and calcium signaling pathway as well as several other pathways, such as fatty acid metabolism, purine and amino acid metabolism (Fig. 7E).

Based on the RNA-Seq results, previous studies also proposed that the

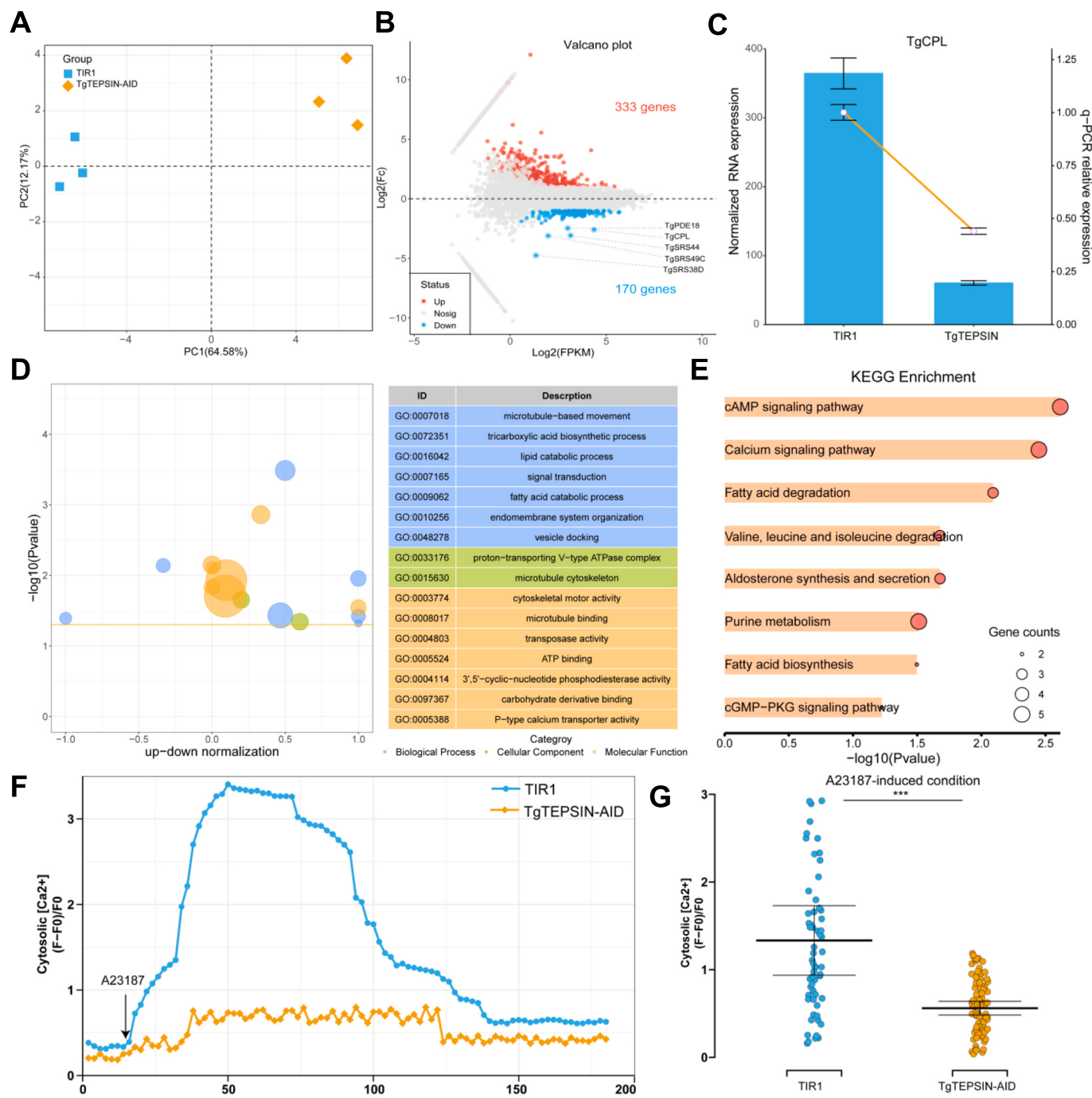


Fig. 7. RNA-Seq comparison between TgTEPSIN-AID fusion line and parental parasites. (A) Principal component analysis (PCA) for all RNA-Seq samples. (B) Volcano plot revealing 333 DEGs with increased expression (red) and 170 with decreased expression (blue) ($P < 0.05$ and $|Log2FC| > 1$). The top 5 genes in the decreased DEGs were marked in the plot. (C) qPCR was used to validate the transcript level of the known PLVAC protease marker TgCPL. (D) The bubble plots show GO enrichment results of the identified DEGs. (E) The bar plot illustrates the enriched KEGG pathways for the identified DEGs. (F) Detection of cytosolic calcium ion levels for the TgTEPSIN-AID parasites and the control TIR1 with IAA induced for 12 h. Representative traces of cytosolic Ca^{2+} measurements in extracellular parasites loaded with the radiometric fluorescent indicator Fluo-4 AM are shown. At the 16 s, 1 μ g/mL A23187 was added to trigger Ca^{2+} release from acidic stores. (G) Quantification of tracings from 3 independent experiments showing the Fluo-4 AM fluorescence for the two parasite lines after A23187 addition. Data ($N = 3$ independent experiments; $n = 3$ replicates) of the above assays shown in the figure are presented as mean \pm SD. Statistical significance was assessed using an unpaired two-tailed Student's *t*-test. *, $P < 0.05$; **, $P < 0.001$; ***, $P < 0.0001$; NS, not significant.

influence of cell invasion and microneme secretion may be attributable to the role of Ca^{2+} fluctuations. Therefore, to explore the role of TgTEPSIN in Ca^{2+} regulation and storage, we measured the cytosolic Ca^{2+} levels in the parental and mutant lines when loaded with the Ca^{2+} -sensitive fluorescent dye Fluo-4 AM. As shown in the temporal

variations of Fig. 7F, the addition of A23187 stimulates calcium release from all compartments of *T. gondii*. Notably, TgTEPSIN-deficient parasites exhibited significantly reduced responsiveness to A23187-induced Ca^{2+} release from acidic compartments (Fig. 7G). This indicates that TgTEPSIN play a crucial role in the Ca^{2+} release or demobilization from

T. gondii.

3.8. Depletion of TgTEPSIN affects bradyzoite differentiation in *T. gondii* ME49

Next, we employed the AID system to generate the TgTEPSIN-AID parasite line based on another background strain *T. gondii* ME49. Obviously, the AID system caused rapid depletion of TgTEPSIN upon treatment with IAA, as indicated by immunofluorescence (Fig. 8A) and immunoblotting analyses (Fig. 8B). Consistent with findings in type I RH strain background, the replication and plaque formation of TgTEPSIN-AID line exhibited a significant reduction in replication efficiency when the addition of IAA, and no significant plaques were formed in host cell monolayers (Fig. 8 C-E).

In addition, the ability of bradyzoite differentiation in the TgTEPSIN-AID parasites incubated with or without IAA was tested by the DBL staining. After incubating the parasites under alkaline condition for 72 and 96 h, most vacuoles with TgTEPSIN-expressing parasites showed strong DBL-positive staining, indicating effective differentiating into the bradyzoite form (Fig. 8F). Quantification of the DBL-positive staining vacuoles confirmed a significant difference in the indicated AID parasite line before and after IAA treatment ($P < 0.05$) (Fig. 8G). Additionally, the bradyzoite specific protein BAG1 was also used to examine the ability of bradyzoite differentiation. Meanwhile, further RT-qPCR analysis confirmed the extremely low expression of BAG1 at 72 and 96 h (Fig. 8H).

4. Discussion

T. gondii differs from other eukaryotic cells by possessing unique secretory organelles, including micronemes, rhoptries, and dense granules, which are sequentially secreted during host cell invasion [37,38]. Building on earlier studies, it is well-established that *T. gondii* possesses a full inventory of endocytic organelles, including endosome-like compartments (ELCs), characterized by Rab5 and Rab7 markers, and the PLVAC, which is defined by CPL and VP1. The endosomal system facilitates vesicular trafficking, regulating the processing and maturation of these secretory organelles [39–42]. The PLVAC plays a key role in the sorting and processing virulence proteins that are essential for the biogenesis of these secretory organelles, and degrades vesicles derived from the endocytic process, which receives host-derived nutrients from the micropore [9,10]. These observations suggest that the PLVAC is unique in its ability to properly transport different vesicles and to form acidified structures. However, the mechanism underlying the uniqueness remains elusive. Here, we leveraged the high efficiency of proximity biotin labeling and CRISPR-tagging techniques in *T. gondii* to identify several novel components of the PLVAC.

It's well known that TgCPL is a type II membrane protein with the N-terminus facing the parasite cytosol and the C-terminus including the catalytic domain facing the PLVAC lumen [43]. As for CRT, it is a homolog of Plasmodium CRT, which is established to have 10 TM domains and have both the N-terminus and C-terminus oriented toward the parasite cytosol [28,44]. As such, the two baits used in our study would only label PLVAC proteins exposed to the parasite cytosol. These orientations are consistent with the identified PLVAC proteins, which are nearly all either multi-pass integral membrane proteins or are likely to be expressed in the parasite cytosol based on the absence of a signal sequence. We acknowledge this as a limitation of the study while also highlighting that the approach was nevertheless successful in identifying novel proteins that are associated with the PLVAC.

The PLVAC appears as a single prominent structure in extracellular parasites, while it evidently appears to be expanded or diffused in the intracellular parasites [14]. This feature suggests that the PLVAC is dynamic and functioning as an organelle for trafficking its components inside parasites as they grow within host cells. In our study, this discrepancy in the PLVAC between the intracellular and extracellular

parasites was also observed with the localization of the newly identified proteins, especially for the important ones, such as VAP30 and VAP34 (Fig. 2E and Fig. S1A). In a previous study, a HyperLOPIT method was applied to identify the spatial proteomics of the extracellular parasite of *T. gondii*, enabling the simultaneous capture of steady-state subcellular locations for thousands of proteins [45]. Based on the predicted results of a large-scale analysis, some known PLVAC markers such as CPL, CPB, ASP1, and CRT were categorized under the "endomembrane vesicles" class, while markers such as AQP1, NHE3, ZNT, and VIT were assigned to the "Golgi" class. Additionally, some newly identified proteins (e.g. VAP12/24/27/32/40) were also predicted to be located within these categories, suggesting their potential proximity to these compartments. In fact, the organelles within the endomembrane system are closely positioned, and this approach cannot precisely predict the exact localization of these proteins but provides useful reference points. These similar features indicated that the potential association of these proteins with the ELCs or the trans-Golgi network.

Among the 9 identified PLVAC proteins in our study, VAP24 and VAP27 have been previously reported in a study on phosphatidylinositol 3-phosphate (PI3P)-binding proteins in *T. gondii* and were named TgPX2 and TgFYVE1, respectively [46]. Notably, while these two proteins have been shown to colocalize with the PLVAC marker TgCPL, they have not yet been conclusively identified or characterized as part of the PLVAC protein repertoire due to the lack of detailed investigation. Additionally, although VAP23 (termed Tepsin) was recently studied for its significance in parasite growth and morphology, its precise localization remains ambiguous [47]. However, in our study, these proteins appeared as candidates in the PLVAC-proximal biotinylated protein list, providing evidence for their potential relevance and warranting further investigation. The STRING database analysis implied predicted functions of the newly identified proteins. Equipped with the essentiality results and conservation analysis, we concentrated on the proteins that contain important domains and conserved homologs in *P. falciparum* (e.g. TgTEPSIN, TgFYVE1, VAP30, and VAP32) caught our attention. As noted, VAP30 contains a magnesium ion transporter-related domain, and it might act in the membrane as metal ion transport in the PLVAC. The findings aligned with previous reports are likely to support the magnesium requirement for the membrane-bound H⁺-PPases [12,48]. Furthermore, FYVE domain of TgFYVE1 are known to specifically bind phosphatidylinositol (PI), enabling its recruitment to the membranes of endosomes and regulating vesicular trafficking [49]. Similarly, TM9SF domain of VAP32, which is widely present in eukaryotes, has been implicated in membrane protein transport and fusion processes, particularly within the intracellular membrane system, such as the endoplasmic reticulum, Golgi apparatus, and lysosomes [50,51]. More knowledge regarding the specific functions of these domains or homologous proteins in *P. falciparum* remains limited and merits further investigation. However, regarding the ENTH domain-containing protein (TgTEPSIN), its homolog in *P. falciparum*, PF3D7_1459600, has been identified with mutations in a whole-genome analysis of artemisinin-resistant strains, implying its potential role in resistance mechanisms in the functionally analogous organelle, the digested vacuole (DV) [52]. In addition, the homolog from *Arabidopsis thaliana*, known as MTV1 (At3g16270) (Table S3), mediates clathrin-dependent trafficking of vacuolar cargo from the trans-Golgi network [53]. Taken together, these preliminary bioinformatic data highlight the significance and necessity in the investigation of TgTEPSIN.

TgTEPSIN acts as a novel PLVAC protein containing the ENTH domain, which has a fitness score of -4.16 and impacts every step of the parasite's life cycle (Fig. 4F). Notably, its effects are comparable to those of the previously published PLVAC protein, VHA1, making it a highly intriguing candidate for further research. Perturbation of the TgTEPSIN function caused major defects in the structural integrity of the PLVAC, suggesting that the protein may be involved in the formation of the organelle by its potential association with vesicle trafficking or fusion of the PLVAC. It is worth noting that TgTEPSIN affects only the secretion of

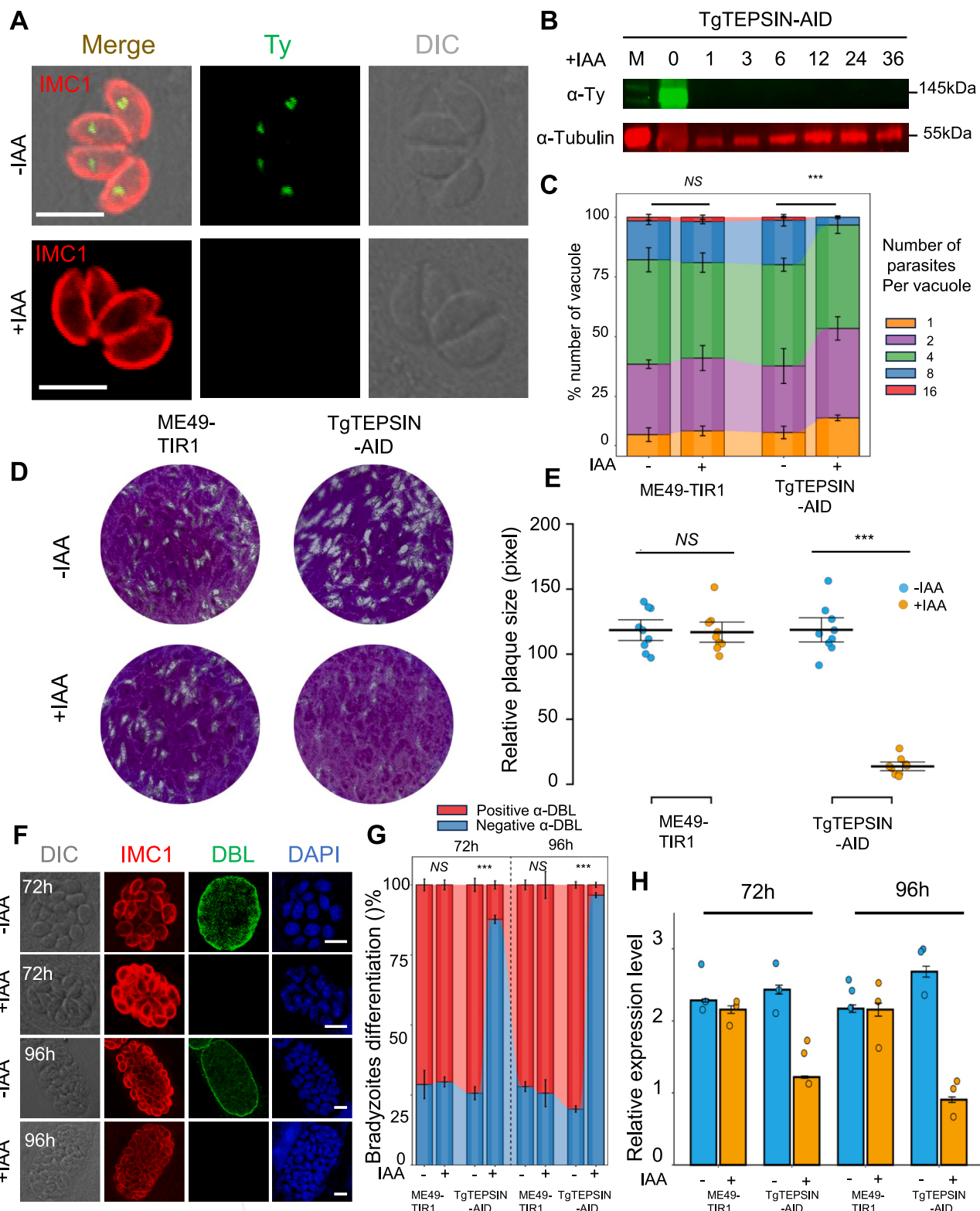


Fig. 8. TgTEPSIN is essential for parasites in the type II strain ME49. (A) IFA identification of TgTEPSIN-AID line using antibodies against the Ty epitope (green) and IMC1 (red). (B) Western blotting analysis of TgTEPSIN-AID line after treating with auxin (IAA) at different time points. (C) Depletion of TgTEPSIN caused the defect in parasite replication. (D, E) Plaque assay was performed to examine the parasite growth. (F) Representative images of the TgTEPSIN-AID parasite lines grown in RPMI-HEPES medium without CO₂ for 3 days for induction of bradyzoites. Red, anti-IMC1; green, FITC-DBL; blue, DAPI. Bar = 5 μ M. The DBL-stained vacuoles of high and middle intensity were all defined as DBL-positive. (G) Quantification of bradyzoite differentiation in the different strains at 72 and 96 h. The percentage of DBL-positive vacuoles was calculated based on at least 200 vacuoles per replicate. (H) The changes in the relative expression level of TgBAG1 at 72 h and 96 h. Bar = 5 μ M. Data (N = 3 independent experiments; n = 3 replicates) from plaque size were shown as the mean \pm SD from at least three in independent biological replicates. For the data from replication and quantification of FITC-DBL staining assays, two-way analysis of variance (ANOVA) with Tukey's multiple comparisons were used, and the data from other assays were tested by the two-tailed, unpaired t-test. *, P < 0.05; **, P < 0.001; ***, P < 0.0001; NS, not significant.

invasion organelles but does not alter their structural morphology. Previous studies suggested that the V-ATPase impacts the processing of MIC and ROP precursor protein and causes morphologic defects on these secretory organelles and PLVAC upon disrupting the V-ATPase. [12,13]. In this study, the strong effect of the TgTEPSIN on the structural maintenance of the PLVAC would affect the secretion of microneme proteins. This information would provide the explanation of why depletion of TgTEPSIN resulted in defects in parasite egress and invasion, as suggested by the defect of microneme secretion. Meanwhile, the additional evidence for the dysfunction of microneme was also supported by the significant changes in Ca^{2+} signaling and cAMP pathway in our RNA-Seq data. Honestly, this potential function of TgTEPSIN in the parasite requires further investigation to clarify and to define the mechanism of the protein in the formation of the PLVAC in *T. gondii*.

The ability of *T. gondii* to transition between the tachyzoite and bradyzoite life stages is crucial for parasite survival and the pathogenesis of toxoplasmosis. In this study, we observed that tachyzoite-to-bradyzoite differentiation was severely impaired in the TgTEPSIN-AID ME49 strain, as evidenced by DBL staining and the reduced expression levels of the bradyzoite marker BAG1. More importantly, the loss of TgTEPSIN in the RH strain resulted in a significant decrease in the relative expression level of TgCPL and structural abnormalities in the PLVAC. TgCPL is a critical cysteine protease within the PLVAC, contributing to its proteolytic activity during the chronic stage and playing a role in the digestion of undigested organelles through autophagy [54]. Previous studies have suggested that autophagy may serve as a potential mechanism to regulate the tachyzoite-to-bradyzoite transformation in *T. gondii* [55,56]. PLVAC acts as a terminal compartment for protein degradation and that TgCPL is strongly associated with TgTEPSIN expression based on our findings. This presents an indirect influence on autophagic processes and stage conversion in *T. gondii*. Additionally, a previous research on another PLVAC marker, TgAAT1, underscored the pivotal role of amino acids in regulating *T. gondii* stage conversion and persistence [25]. Meanwhile, cyclic nucleotide kinases from cAMP or cGMP signaling pathways have also been reported to inhibit replication and induce differentiation in *T. gondii* [57]. Our current findings indicate that the depletion of TgTEPSIN indeed impacts these related pathways, as suggested by RNA-seq results. Further in-depth experiments are needed to validate these connections and explore the role of TgTEPSIN in stage conversion from additional perspectives, thereby enhancing our understanding of PLVAC functionality. Undeniably, ME49 strain is widely recognized as a reliable model for studying in vitro stage differentiation, with the ability to form bradyzoites and cysts. However, it may be less efficient under certain in vivo and vitro conditions compared to the Pru strain, which is frequently employed in most studies on bradyzoite differentiation and cyst formation. Despite this limitation, the preliminary transformation experiments in this study provide valuable insights. Further vivo experiments in mice using the Pru strain will help to provide more comprehensive and definitive conclusions.

Eukaryotic cells contain four distinct adaptins (AP) complexes, each responsible for targeting specific organelles, thus determining their roles in cargo transport and function [58–60]. *T. gondii* retains all genes encoding proteins/subunits of the AP1, AP2, AP3, and AP4 complexes in its genome [61]. Previous studies have underscored the significance of the AP1 complex, implicating the TgAp1 subunit and TgEpsl in vesicle trafficking at the Golgi apparatus and trans-Golgi network in the parasite [62]. Intriguingly, a previous study identified the beta subunit of the AP2 complex functioning at the Golgi apparatus for vesicle trafficking, yet other subunits of the complex act at the micropore for endocytosis [6]. This suggests that subunits of the AP complexes are divergent. This feature in the parasite was further supported by identification of TgTEPSIN at the PLVAC in this study, particularly as other subunits of the AP4 complex were localized to the Golgi apparatus [58]. Therefore, the essential protein TgTEPSIN identified in this study provides another opportunity to investigate the evolution of the parasite in the

apicomplexans, and to understand the specialization of the PLVAC and potentially its closely related organelle, i.e. the food vacuole in *P. falciparum*. Future studies are needed to define the precise role of the protein and its interacting partners in the specialized organelle – the PLVAC in *T. gondii* and the closely related protists.

Supplementary data to this article can be found online at <https://doi.org/10.1016/j.ijbiomac.2025.140311>.

CRediT authorship contribution statement

Kai He: Writing – original draft, Methodology, Investigation. **Ruixin Wu:** Writing – original draft, Methodology, Investigation. **An Yan:** Methodology, Investigation, Formal analysis. **Xianyong Liu:** Writing – review & editing, Supervision. **Shaojun Long:** Writing – review & editing, Supervision, Funding acquisition.

Informed consent statement

Not applicable.

Funding

This research was supported by the National Key Research and Development Program of China (2022YFD1800200).

Declaration of competing interest

The authors declare no conflict of interest

Acknowledgments

We are grateful to the imaging center at the Institute of Food Science and Technology, CAAS, for assistance with the TEM. We also thank Prof. Vern Carruthers for generously providing the RHΔku80Δhxgprt line, Prof. David Sibley for the kind gifts of antibodies against MIC2, SAG1 (DG52), GRA7 and ROP5, and the TIR1 background line and the corresponding plasmids, and Prof. Philippe Bastin for BB2 monoclonal antibodies against the Ty epitope tag. We are also grateful to Prof. Jin-Lei Wang (Lanzhou Veterinary Research Institute, Chinese Academy of Agricultural Sciences) for providing an antibody against HSP60.

Data availability

The raw transcriptomic data and proteomic data reported in this paper have been deposited in the Genome Sequence Archive (GSA, <https://ngdc.cncb.ac.cn/gsa/>) and OMIX (<https://ngdc.cncb.ac.cn/omix/>), China National Center for Bioinformation/Beijing Institute of Genomes, China Academy of Sciences with accession number CRA017570 and OMIX006797, respectively.

References

- [1] M. Attias, D.E. Teixeira, M. Benchimol, R.C. Vommaro, P.H. Crepaldi, W. De Souza, The life-cycle of toxoplasma gondii reviewed using animations, *Parasit. Vectors* 13 (1) (2020) 588.
- [2] B. Shen, Genetic Manipulation Toolkits in Apicomplexan Parasites, *Zoonoses*, 2022.
- [3] H. Dong, R. Su, Y. Lu, M. Wang, J. Liu, F. Jian, Y. Yang, Prevalence, risk factors, and genotypes of toxoplasma gondii in food animals and humans (2000–2017) from China, *Front. Microbiol.* 9 (2018) 2108.
- [4] Z. Dou, O.L. McGovern, M. Di Cristina, V.B. Carruthers, *Toxoplasma gondii* ingests and digests host cytosolic proteins, *mBio* 5 (4) (2014) e01188–01114.
- [5] R.B. Guevara, B.A. Fox, D.J. Bzik, Toxoplasma gondii parasitophorous vacuole membrane-associated dense granule proteins regulate maturation of the cyst wall, *MSphere* 5 (1) (2020) 101128.
- [6] W. Wan, H. Dong, D.H. Lai, J. Yang, K. He, X. Tang, Q. Liu, G. Hide, X.Q. Zhu, L. D. Sibley, et al., The toxoplasma micropore mediates endocytosis for selective nutrient salvage from host cell compartments, *Nat. Commun.* 14 (1) (2023) 977.
- [7] Q.Q. Wang, M. Sun, T. Tang, D.H. Lai, J. Liu, S. Maity, K. He, X.T. Wu, J. Yang, Y. B. Li, et al., Functional screening reveals toxoplasma prenylated proteins required

- for endocytic trafficking and rhoptry protein sorting, *mBio* 14 (4) (2023) e0130923.
- [8] K. He, Q. Wang, X. Gao, T. Tang, H. Ding, S. Long, Transcriptomic and metabolomic analyses reveal the essential nature of Rab1B in toxoplasma gondii, *Parasit. Vectors* 16 (1) (2023) 409.
- [9] A.J. Stasic, S.N.J. Moreno, V.B. Carruthers, Z. Dou, The toxoplasma plant-like vacuolar compartment (PLVAC), *J. Eukaryot. Microbiol.* 69 (6) (2022) e12951.
- [10] O.L. McGovern, Y. Rivera-Cuevas, V.B. Carruthers, Emerging mechanisms of endocytosis in toxoplasma gondii, *Life (Basel)* 11 (2) (2021).
- [11] J. Huotari, A. Helenius, Endosome maturation, *EMBO J.* 30 (17) (2011) 3481–3500.
- [12] J. Liu, D. Pace, Z. Dou, T.P. King, D. Guidot, Z.H. Li, V.B. Carruthers, S.N. Moreno, A vacuolar-H⁺-pyrophosphatase (TgVP1) is required for microneme secretion, host cell invasion, and extracellular survival of toxoplasma gondii, *Mol. Microbiol.* 93 (4) (2014) 698–712.
- [13] A.J. Stasic, N.M. Chasen, E.J. Dykes, S.A. Vella, B. Asady, V.J. Starai, S.N. J. Moreno, The toxoplasma vacuolar H⁺-ATPase regulates intracellular pH and impacts the maturation of essential secretory proteins, *Cell Rep.* 27 (7) (2019) 2132–2146 e2137.
- [14] F. Parussini, I. Coppens, P.P. Shah, S.L. Diamond, V.B. Carruthers, Cathepsin L occupies a vacuolar compartment and is a protein maturase within the endo/exocytic system of toxoplasma gondii, *Mol. Microbiol.* 76 (6) (2010) 1340–1357.
- [15] Z. Dou, V.B. Carruthers, Cathepsin proteases in toxoplasma gondii, *Adv. Exp. Med. Biol.* 712 (2011) 49–61.
- [16] L.B. Thornton, M. Key, C. Micchelli, A.J. Stasic, S. Kwain, K. Floyd, S.N. Moreno, B. N. Dominy, D.C. Whitehead, Z. Dou, A cathepsin C-like protease mediates the post-translational modification of Toxoplasma gondii secretory proteins for optimal invasion and egress, *Mbio* 14 (4) (2023) e00174–23.
- [17] T. Boller, H. Kende, Hydrolytic enzymes in the central vacuole of plant cells, *Plant Physiol.* 63 (6) (1979) 1123–1132.
- [18] K. Miranda, D.A. Pace, R. Cintron, J.C. Rodrigues, J. Fang, A. Smith, P. Rohloff, E. Coelho, F. de Haas, W. de Souza, et al., Characterization of a novel organelle in toxoplasma gondii with similar composition and function to the plant vacuole, *Mol. Microbiol.* 76 (6) (2010) 1358–1375.
- [19] N.M. Chasen, A.J. Stasic, B. Asady, I. Coppens, S.N. Moreno, The vacuolar zinc transporter TgZnT1 protects Toxoplasma gondii from zinc toxicity, *MspHERE* 4 (3) (2019), 00086–19.
- [20] D. Aghabi, M. Sloan, G. Gill, E. Hartmann, O. Antipova, Z. Dou, A.J. Guerra, V. B. Carruthers, C.R. Harding, The vacuolar iron transporter mediates iron detoxification in toxoplasma gondii, *Nat. Commun.* 14 (1) (2023) 3659.
- [21] M.E. Francia, S. Wicher, D.A. Pace, J. Sullivan, S.N. Moreno, G. Arribalzaga, A toxoplasma gondii protein with homology to intracellular type Na⁺/H⁺ exchangers is important for osmoregulation and invasion, *Exp. Cell Res.* 317 (10) (2011) 1382–1396.
- [22] S. Luo, M. Vieira, J. Graves, L. Zhong, S.N. Moreno, A plasma membrane-type Ca²⁺-ATPase co-localizes with a vacuolar H⁺-pyrophosphatase to acidocalcisomes of Toxoplasma gondii, *EMBO J.* 20 (2) (2001) 55–64.
- [23] S. Luo, F.A. Ruiz, S.N. Moreno, The acidocalcisome Ca²⁺-ATPase (TgA1) of toxoplasma gondii is required for polyphosphate storage, intracellular calcium homeostasis and virulence, *Mol. Microbiol.* 55 (4) (2005) 1034–1045.
- [24] B. Asady, C.F. Dick, K. Ehrenman, T. Sahu, J.D. Romano, I. Coppens, A single Na⁺/Pi cotransporter in toxoplasma plays key roles in phosphate import and control of parasite osmoregulation, *PLoS Pathog.* 16 (12) (2020) e1009067.
- [25] F. Piro, S. Masci, G. Kannan, R. Focaia, T.L. Schultz, P. Thaprawat, V.B. Carruthers, M. Di Cristina, A Toxoplasma gondii putative amino acid transporter localizes to the plant-like vacuolar compartment and controls parasite extracellular survival and stage differentiation, *MspHERE* 9 (1) (2024) e00597–23.
- [26] L.B. Thornton, P. Teehan, K. Floyd, C. Cochrane, A. Bergmann, B. Riegel, A. J. Stasic, M. Di Cristina, S.N.J. Moreno, P.D. Roepke, et al., An ortholog of plasmodium falciparum chloroquine resistance transporter (PfCRT) plays a key role in maintaining the integrity of the endolysosomal system in toxoplasma gondii to facilitate host invasion, *PLoS Pathog.* 15 (6) (2019) e1007775.
- [27] G. Kannan, M. Di Cristina, A.J. Schultz, M.H. Huynh, F. Wang, T.L. Schultz, M. Lunghi, I. Coppens, V.B. Carruthers, Role of toxoplasma gondii chloroquine resistance transporter in bradyzoite viability and digestive vacuole maintenance, *mBio* 10 (4) (2019).
- [28] S.D. Warring, Z. Dou, V.B. Carruthers, G.I. McFadden, G.G. van Dooren, Characterization of the chloroquine resistance transporter homologue in toxoplasma gondii, *Eukaryot. Cell* 13 (11) (2014) 1360–1370.
- [29] S. Long, Q. Wang, L.D. Sibley, Analysis of noncanonical calcium-dependent protein kinases in toxoplasma gondii by targeted gene deletion using CRISPR/Cas9, *Infect. Immun.* 84 (5) (2016) 1262–1273.
- [30] K.M. Brown, S. Long, L.D. Sibley, Plasma membrane association by N-acylation governs PKG function in toxoplasma gondii, *mBio* 8 (3) (2017).
- [31] S. Long, K.M. Brown, L.L. Drewry, B. Anthony, I.Q.H. Phan, L.D. Sibley, Calmodulin-like proteins localized to the conoid regulate motility and cell invasion by toxoplasma gondii, *PLoS Pathog.* 13 (5) (2017) e1006379.
- [32] D. Soldati, J.C. Boothroyd, Transient transfection and expression in the obligate intracellular parasite toxoplasma gondii, *Science* 260 (5106) (1993) 349–352.
- [33] S. Long, K.M. Brown, L.D. Sibley, CRISPR-mediated tagging with BirA allows proximity labeling in toxoplasma gondii, *Bio-Protoc.* 8 (6) (2018).
- [34] Z. Shan, X. Song, X. Yang, Y. Xue, Y. Wu, X. Wang, J. Liu, Q. Liu, Calreticulin (CALR) promotes ionophore-induced microneme secretion in toxoplasma gondii, *Parasitol. Res.* 123 (2) (2024) 139.
- [35] L. Pernas, C. Bean, J.C. Boothroyd, L. Scorrano, Mitochondria restrict growth of the intracellular parasite toxoplasma gondii by limiting its uptake of fatty acids, *Cell Metab.* 27 (4) (2018) 886–897.e884.
- [36] H. Dong, J. Yang, K. He, W.B. Zheng, D.H. Lai, J. Liu, H.Y. Ding, R.B. Wu, K. M. Brown, G. Hide, et al., The toxoplasma monocarboxylate transporters are involved in the metabolism within the apicoplast and are linked to parasite survival, *eLife* (2024) 12.
- [37] S.M. Sidik, D. Huet, S.M. Ganesan, M.H. Huynh, T. Wang, A.S. Nasamu, P. Thiru, J. P.J. Saeij, V.B. Carruthers, J.C. Niles, et al., A genome-wide CRISPR screen in toxoplasma identifies essential apicomplexan genes, *Cell* 166 (6) (2016) 1423–1435 e1412.
- [38] L. Sheiner, D. Soldati-Favre, Protein trafficking inside toxoplasma gondii, *Traffic* 9 (5) (2008) 636–646.
- [39] P.J. Sloves, S. Delhayé, T. Mouveaux, E. Werkmeister, C. Slomiany, A. Hovasse, T. Dilezikto Alayi, I. Callebaut, R.Y. Gajj, C. Schaeffer-Reiss, et al., Toxoplasma sortilin-like receptor regulates protein transport and is essential for apical secretory organelle biogenesis and host infection, *Cell Host Microbe* 11 (5) (2012) 515–527.
- [40] K. Kremer, D. Kamin, E. Rittweger, J. Wilkes, H. Flammer, S. Mahler, J. Heng, C. J. Tonkin, G. Langley, S.W. Hell, et al., An overexpression screen of toxoplasma gondii Rab-GTPases reveals distinct transport routes to the micronemes, *PLoS Pathog.* 9 (3) (2013) e1003213.
- [41] J. Morlon-Guyot, S. Pastore, L. Berry, M. Lebrun, W. Daher, Toxoplasma gondii Vps11, a subunit of HOPS and CORVET tethering complexes, is essential for the biogenesis of secretory organelles, *Cell. Microbiol.* 17 (8) (2015) 1157–1178.
- [42] L.O. Sangaré, T.D. Alayi, B. Westermann, A. Hovasse, F. Sindikubwabo, I. Callebaut, E. Werkmeister, F. Lafont, C. Slomiany, M.A. Hakimi, et al., Unconventional endosome-like compartment and retromer complex in toxoplasma gondii govern parasite integrity and host infection, *Nat. Commun.* 7 (2016) 11191.
- [43] E.T. Larson, F. Parussini, M.H. Huynh, J.D. Giebel, A.M. Kelley, L. Zhang, M. Bogyo, E.A. Merritt, V.B. Carruthers, Toxoplasma gondii cathepsin L is the primary target of the invasion-inhibitory compound morpholinurea-leucyl-homophenyl-vinyl sulfone phenyl, *J. Biol. Chem.* 284 (39) (2009) 26839–26850.
- [44] R.E. Martin, K. Kirk, The malaria parasite's chloroquine resistance transporter is a member of the drug/metabolite transporter superfamily, *Mol. Biol. Evol.* 21 (10) (2004) 1938–1949.
- [45] K. Baryluk, L. Koreny, H. Ke, S. Butterworth, O.M. Crook, I. Lassadi, V. Gupta, E. Tromer, T. Mourier, T.J. Stevens, et al., A comprehensive subcellular atlas of the toxoplasma proteome via hyperLOPIT provides spatial context for protein functions, *Cell Host Microbe* 28 (5) (2020) 752–766 e759.
- [46] W. Daher, J. Morlon-Guyot, L. Sheiner, G. Lentini, L. Berry, L. Tawk, J. F. Dubremetz, K. Wengelnik, B. Striepen, M. Lebrun, Lipid kinases are essential for apicoplast homeostasis in toxoplasma gondii, *Cell. Microbiol.* 17 (4) (2015) 559–578.
- [47] R.R. Pasquarelli, J.J. Quan, E.S. Cheng, V. Yang, T.A. Britton, J. Sha, J. A. Wohlschlegel, P.J. Bradley, Characterization and functional analysis of Toxoplasma Golgi-associated proteins identified by proximity labeling, *mBio* 15 (11) (2024) e02380–24.
- [48] A.A. Baykov, N.P. Bakuleva, P.A. Rea, Steady-state kinetics of substrate hydrolysis by vacuolar H⁺-pyrophosphatase. A simple three-state model, *Eur. J. Biochem.* 217 (2) (1993) 755–762.
- [49] C. Liu, Y. Zeng, H. Li, C. Yang, W. Shen, M. Xu, Z. Xiao, T. Chen, B. Li, W. Cao, et al., A plant-unique ESCRT component, FYVE4, regulates multivesicular endosome biogenesis and plant growth, *New Phytol.* 231 (1) (2021) 193–209.
- [50] B. Pruvot, V. Laurens, F. Salvadori, E. Solary, L. Pichon, J. Chluba, Comparative analysis of nonspanin protein sequences and expression studies in zebrafish, *Immunogenetics* 62 (10) (2010) 681–699.
- [51] A. Vernay, O. Lamrabet, J. Perrin, P. Cosson, TM9SF4 levels determine sorting of transmembrane domains in the early secretory pathway, *J. Cell Sci.* 131 (21) (2018).
- [52] F. Ariey, B. Witkowski, C. Amarantunga, J. Beghain, A.C. Langlois, N. Khim, S. Kim, V. Duru, C. Bouchier, L. Ma, et al., A molecular marker of artemisinin-resistant plasmodium falciparum malaria, *Nature* 505 (7481) (2014) 50–55.
- [53] M. Sauer, M.O. Delgado, J. Zouhar, G.D. Reynolds, J.G. Pennington, L. Jiang, S. J. Liljegren, Y.D. Stierhof, G. De Jaeger, M.S. Otegui, et al., MTV1 and MTV4 encode plant-specific ENTH and ARF GAP proteins that mediate clathrin-dependent trafficking of vacuolar cargo from the trans-Golgi network, *Plant Cell* 25 (6) (2013) 2217–2235.
- [54] M. Di Cristina, Z. Dou, M. Lunghi, G. Kannan, M.H. Huynh, O.L. McGovern, T. L. Schultz, A.J. Schultz, A.J. Miller, B.M. Hayes, et al., Toxoplasma depends on lysosomal consumption of autophagosomes for persistent infection, *Nat. Microbiol.* 2 (2017) 17096.
- [55] X. Li, D. Chen, Q. Hua, Y. Wan, L. Zheng, Y. Liu, J. Lin, C. Pan, X. Hu, F. Tan, Induction of autophagy interferes the tachyzoite to bradyzoite transformation of toxoplasma gondii, *Parasitology* 143 (5) (2016) 639–645.
- [56] D. Smith, G. Kannan, I. Coppens, F. Wang, H.M. Nguyen, A. Cerutti, E.B. Olafsson, P.A. Rimple, T.L. Schultz, N.M. Mercado Soto, et al., Toxoplasma TgATG9 is critical for autophagy and long-term persistence in tissue cysts, *eLife* 10 (2021).
- [57] M.S. Eaton, L.M. Weiss, K. Kim, Cyclic nucleotide kinases and tachyzoite-bradyzoite transition in toxoplasma gondii, *Int. J. Parasitol.* 36 (1) (2006) 107–114.
- [58] T.L. Archuleta, M.N. Frazier, A.E. Monken, A.K. Kendall, J. Harp, A.J. McCoy, N. Creanza, L.P. Jackson, Structure and evolution of ENTH and VHS/ENTH-like domains in tepsin, *Traffic* 18 (9) (2017) 590–603.
- [59] A. Sanger, J. Hirst, A.K. Davies, M.S. Robinson, Adaptor protein complexes and disease at a glance, *J. Cell Sci.* 132 (20) (2019).

- [60] J. Birnbaum, S. Scharf, S. Schmidt, E. Jonscher, W.A.M. Hoeijmakers, S. Flemming, C.G. Toenhake, M. Schmitt, R. Sabitzki, B. Bergmann, et al., A Kelch13-defined endocytosis pathway mediates artemisinin resistance in malaria parasites, *Science* 367 (6473) (2020) 51–59.
- [61] W.D. Nevin, J.B. Dacks, Repeated secondary loss of adaptin complex genes in the Apicomplexa, *Parasitol. Int.* 58 (1) (2009) 86–94.
- [62] K. Venugopal, E. Werkmeister, N. Barois, J.M. Saliou, A. Poncet, L. Huot, F. Sindikubwabo, M.A. Hakimi, G. Langsley, F. Lafont, et al., Dual role of the *Toxoplasma gondii* clathrin adaptor AP1 in the sorting of rhoptry and microneme proteins and in parasite division, *PLoS Pathog.* 13 (4) (2017) e1006331.